BELLCOMM, INC.
1100 SEVENTEENTH STREET, N.W. WASHINGTON, D.C. 20036

COVER SHEET FOR TECHNICAL MEMORANDUM

TITLE- Surface Temperatures, Accelerations and Loads Encountered by Spherical Bodies Entering from Near-Earth Orbits

TM- 67-2033-2

DATE- March 28, 1967

FILING CASE NO(S)- 330

AUTHOR(S)- J. Jellinek

FILING SUBJECT(S)- (ASSIGNED BY AUTHOR(S)- Spherical Body Entry Conditions and Application to Orbital Escape Devices

ABSTRACT

A study was made of entry heating, acceleration and loading conditions for several spheres. These were 7, 20 and 58.5 feet in diameter. Total weights of 500 and 680 pounds were considered.

Metallic fabric thickness, temperature limitations and the effects of deceleration during entry on inflated spherical structures also were examined. The results were reviewed to estimate practical size ranges for entering spherical escape devices.

It was found that spherical bodies are presently not good candidates for escape devices: The spherical shells would require ablative coating on the entire surface; rigid spherical shells create a storage problem; use of metallic fabric with its current temperature limitation of 2000°F would necessitate balloons larger than 20 feet and, would therefore, limit fabric skin thicknesses to less than 5 thousandths of an inch. This, would entail the risk of tearing during unfolding and entry by astronaut.

A literature search covering air radiation and emission off metallic surfaces is reported in Appendix A. An investigation of the chemical reaction of air germaine to entry phenomena is discussed in Appendix B.

[redacted] (ACCESSION NUMBER) 53
X67-71234 (THRU) 2A

(NASA-CR-154366) SURFACE TEMPERATURES, ACCELERATIONS AND LOADS ENCOUNTERED BY SPHERICAL BODIES ENTERING FROM NEAR-EARTH ORBITS (Bellcomm, Inc.) 53 p

N79-71952

Unclas
00/13 12453

SEE REVERSE SIDE FOR DISTRIBUTION LIST

BELLCOMM, INC.

SUBJECT: Surface Temperatures, Accelerations and Loads Encountered by Spherical Bodies Entering from Near-Earth Orbits - Case 330

DATE: March 28, 1967

FROM: J. Jellinek

TM-67-2033-2

TECHNICAL MEMORANDUM

Introduction

Reference [1]* reported a proposal for a balloon type rescue vehicle for emergency entry from earth orbit. This proposal appeared promising because of its simplicity of design and operation and the minimum need for astronaut participation. It was suggested that a large balloon made of metallic fabric would provide so much drag that ablative or other cooling systems would not be necessary. To check the validity of this premise a study was made of entry heating conditions for several spheres. Three spherical bodies were considered: a 7 foot diameter, 680 pound sphere; a 20 foot diameter, 680 pound sphere; and a 58.5 foot diameter, 680 pound sphere. (For comparison purposes the entry trajectory of a one foot diameter, 327 pound sphere was also calculated and plotted.) The study involved the determination of the trajectory parameters (altitude, velocity, inclination angle and time), the determination of stagnation temperatures in the continuum flow regions, and the determination of the leading edge surface temperatures.

Metallic fabric skin thickness, temperature limitations and the effects of deceleration during entry on spherical structures also were examined. The results were reviewed to estimate practical size ranges for entering spherical escape devices. These results and those of similar calculations for 500 pound spheres are shown in Figure 9.

Discussion of Results

Referring to Figure 2 it can be seen that the time from beginning of entry to slow down to a given instantaneous velocity is the same for the three spheres selected for comparison. This is because the instantaneous inclination angle for the entering spheres (see Figure 4) is the same at any given, instantaneous, velocity. However, the altitude of the spheres, at a given velocity, varies with B, the ballistic coefficient. For example, at a velocity of 0.4 x orbital velocity ($V/V_f = 0.4$), the B = 8.84 psf, 7 foot diameter sphere and the B = 285 psf, 1 foot diameter sphere are separated in altitude by 80,000 feet. At

*Numbers in brackets refer to references at the end of the report.

the same velocity, 100,000 feet separate the B = 0.1276 psf, 58.5 foot diameter sphere from the 7 foot diameter sphere.

Comparing Figures 5 and 6 which show stagnation and surface temperatures, respectively, it may be seen that radiation cooling significantly lowers the leading edge wall temperatures. For instance, the maximum skin temperatures found on the 58.5, 20 and 7 foot diameter (680 lb) spheres were 1888°R (1428°F), 2440°R (1980°F) and 3640°R (3180°F), respectively. This occurred while the dissociated air in the shock region was at 8300°R (7840°F), 9330°R (8870°F) and 10,520°R (10,060°F), respectively. From Figure 9 it may be seen that the sharpest drop-off in maximum skin temperatures occur in going from a 7 foot to a 20 foot diameter sphere and that the curves flatten for further increases in sphere diameter. A practical limitation on the use of metallic fabric for spherical structures may be derived by considering the thickness and weight of the skin material. If 250 pounds is allocated to skin weight for 500 and 680 pound spheres and a skin fabric thickness equivalent to .005 stainless steel sheet is assumed, then 20 feet is the maximum possible sphere diameter. While spheres of Tungsten, Columbiun, Tantalum or Molybdenum coated sheet could stand up to 3500°F, suitably coated fabrics of these materials are limited to approximately 2000°F. This is because of the catastrophic oxidation of the fine metallic strands that make up the yarns which, in turn, are woven into the fabric. The coated metallic strands simply flash and burn above 2000°F in air.

Coating either rigid or inflatable shells with ablative material will enable the shells to survive reentry. Since the skin weight of a spherical shell increases with the square of its diameter, consideration of the weight of the required ablative coating suggests use of a small, comparatively dense sphere for an entry device. For instance, the weights involved in coating 7 foot and 20 foot spheres with 0.250 inch layers of phenolic nylon ablator material are 240 pounds and 1958 pounds, respectively. Use of an ablative coated sphere larger than approximately 7 feet appears prohibitive from the weight standpoint. A sphere with aerodynamic directionality, i.e., trimmed with the c.g. forward of the center of volume, would allow ablative material to be added only on the forward surface and thus would save overall weight. This aerodynamic directionality is, however, much easier to achieve with shapes other than spheres. From the above considerations (e.g., storage, directionality and temperature limitations) it would appear that spheres are not good candidates for escape devices. However, it may be seen in Figure 9 that if a metallic fabric that can withstand 2500°F can be developed, then balloon type rescue vehicles might, indeed, be feasible for low altitude earth orbits.

A remaining reason against the use of metallic spheres for rescue devices is their lack of "growth" capability for entry from higher orbits. An approach is to consider the changes necessary in the thermal protection used on a rescue device orginally designed for low earth orbit entry (up to 200 n.m.) to permit its use for entry from a 2000 n. miles orbit or from a synchronous orbit, i.e., 19,350 n. miles altitude.* The spacecraft will be traveling at 28,000 ft/sec when entering from a 2000 n. miles circular orbit and at 33,800 ft/sec when entering from a 19,350 n. miles orbit. It may be seen from Figure A-9 that there is a very large increase in the non-equilibrium "luminous front" radiation in going from a 26,000 ft/sec to a 33,800 ft/sec entry velocity. The surface temperature will increase considerably and will clearly exceed the structural limits of Tungsten, Columbium or Tantalum fabric (already marginal for low earth orbit entries) even if a suitable coating were found for oxidation protection. The same consideration would apply to reentry from a highly elliptical earth orbit. By contrast, an entry device using an ablative shield would require only a thicker coating of ablative material to enable entry from a higher altitude orbit. Such a rescue vehicle originally designed with a thickness of ablative material for, say, a 32,000 ft/sec entry velocity would certainly work for a 26,000 ft/sec entry.

Trajectory Determination

Altitude vs. Speed and Inclination vs. Speed Computations

The trajectories of the three selected spheres were determined by the use of the equations developed by Loh, [2]. When the lift to drag ratio, L/D, is zero, as in the case of a sphere, the trajectory becomes a non-lifting ballistic entry and the applicable equations become,

$$\cos\Theta = \frac{\cos\Theta_f}{1 + \left(\frac{1}{\beta R_o}\right)\left(\frac{gR_o}{V^2} - 1\right)\left(1 - \frac{\rho_f}{\rho}\right)} \tag{1}$$

and

$$\ln\left(\frac{V_f}{V}\right)^2 = \frac{\frac{\rho(gR_o)}{B}\,(\Theta - \Theta_f)}{\cos\Theta\left(\frac{gR_o}{V^2} - 1\right)} \tag{2}$$

*Significant changes in retro-propulsion capability would also be needed.

where

θ, θ_f = instantaneous angle of inclination to horizontal and angle of inclination to horizontal at beginning of unpowered glide, respectively; degrees, positive for descent

β = constant in planetary density vs. altitude relation, $P=P_o\ e^{-\beta h}$ (P_o = 0.0027 slugs/ft^3; $\frac{1}{\beta}$ = 23,500 for earth)

R_o = radius of earth, ft

g = acceleration due to gravity, ft/sec^2

ρ,ρ_f = instantaneous atmospheric density and atmospheric density at beginning of unpowered entry, respectively, slugs/ft^3

B = ballistic coefficient mg/C_DA, lbs/ft^2

V,V_f = instantaneous velocity and velocity at beginning of unpowered entry, respectively, ft/sec

One notes that since the equations are coupled, an explicit answer for the values of θ and V_f/V cannot be obtained. Therefore, an iterative numerical technique must be used before actual values for the variables can be determined. The iterative process, however, is not too cumbersome since the instantaneous angle of inclination, θ, remains close to zero for the first 1/4 of the entry phase and does not become significant until half the speed is expended. By that time a prediction pattern is developed and only 3 or 4 assumptions for θ and V, at a given altitude, are necessary before the iterated values converge to the desired accuracies.

The only place where the size and weight of the sphere enters, is in the ballistic coefficient B in Equation (2). B is found from

$$B = \frac{mg}{C_DA}$$

where

m = mass, slugs

g = acceleration of gravity, ft/sec^2

C_D= drag coefficient = $2D/\rho V^2A$, dimensionless

A = entry vehicle reference area, ft^2. (For a sphere $A=\Pi R^2$.)

The drag coefficient C_D for a sphere in hypersonic flow depends weakly on Reynolds number, Re, for Re>100. This may be seen in Figure 1. For this exercise, values of C_D=1.1, 1.03 and 1.0 were chosen for the 7 foot, 20 foot and 58.5 foot spheres, respectively. This is because the Reynolds number behind a normal shock was calculated to be approximately 159, 454 and 1330 for the 7 foot, 20 foot and 58.5 foot sphere, respectively, at 300,000 feet. Accordingly, B was found to be 8.84 psf for the case of a 680 pound, 7 foot sphere; 1.082 psf for the case of a 680 pound, 20 foot sphere; and 0.1276 psf for the case of a 680 pound, 58.5 foot sphere. (For the 1 foot, 327 pound sphere a C_D = 1.46 was used since Re≈10, and this gave a ballistic coefficient B of 285 psf.)

The results of the altitude vs. speed computations are plotted in Figure 2. For these plots use was made of the air properties of [3].

It may be concluded from an examination of Figure 2 that the large diameter sphere remains at a higher altitude while it is losing speed. However, with a larger size sphere the transition from free molecular flow to continuum flow occurs at a higher altitude. This point of transition depends on the mean free path of the molecules between collisions and on the characteristic length of the body as expressed by the Knudsen number $K=\lambda/D$ where λ is the mean free path and D is the diameter of the sphere for this exercise. Since the mean free path varies inversely with the density of the air, it is large at high altitude. Therefore, a larger body must be at a higher altitude than a smaller body for the same value of K. Prof. Tsien, [4], has chosen the boundaries of the flow regimes of fluids - continuum flow, transition flow and free molecular flow - to be $K \leq 1/100$, $1/100 < K \leq 10$, and $K > 10$, respectively. In the continuum region, gas dynamics relations hold. In the transition regime, second order effects have to be considered in the Navier-Stokes equations in order to handle, mathematically, the phenomena of "slip". In the free molecular region, direct collisions between the body and air molecules take place and kinetic theory has to be used to find temperatures. While effects in the transition and free molecular region would have to be considered in specific entry body designs, these effects would not significantly affect the conclusions of this study.

Figure 4 shows the results of the angle of inclination vs. speed computations. It should be noted that the instantaneous angle of entry is the same for all spheres at any particular speed. This is so because L/D=0 for all spheres. (The inclination angle would not be the same at any particular speed for all bodies with an L/D=1 because an additional term involving L/D and C_D would be present.)

Time vs. Velocity Computations

To find time measured from the beginning of unpowered entry a force balance for the model in Figure 3 was developed. From a consideration of the forces acting on the vehicle, the equations of motion may be written as

$$\frac{dV}{dt} = g \sin \Theta - (D/m) \tag{3}$$

and

$$V(d\Theta/dt) = [g-(V^2/R)] \cos \Theta -(L/m) \tag{4}$$

In Eq. (3) the acceleration tangent to the flight path is equated to the component of gravitational acceleration acting along the flight path and to the drag deceleration. Equation (4) is the force balance in the direction perpendicular to the flight path, in which the contributions per unit mass of lift, gravity, and centrifugal forces are set equal to the centripetal acceleration of the body.

If it is assumed that (a) the acceleration of gravity is constant (R is approximately constant), and (b) the drag force D is constant, then Eqs (3) and (4) become

$$\frac{dV}{dt} = 32.2 \sin \Theta - (D/m) \tag{5}$$

and

$$V \frac{d\Theta}{dt} = [32.2 - (V^2/21.6\times10^6)] \cos \Theta \tag{6}$$

(The last term on the right hand side of Eq. (4) is zero since for a sphere the lift force, L, is zero.) Numerical integration results in,

$$\Delta t = \frac{V\Delta\Theta}{\cos \Theta \; [32.2 - V^2/21.6\times10^6)]} . \tag{7}$$

For this exercise, $\Theta=0$ when $t=0$. Therefore, it is merely necessary to add Δ t's - corresponding to the Δ Θ's found from Eqs. (1) and (2) - to find the time, t, elapsed since the start of unpowered entry. Selected values of time, t, are shown in Figure 2 for the two spherical shells.

Temperature Determination

Stagnation Point Temperature Determination

Stagnation point temperatures, corresponding to the speeds and altitudes calculated by Eqs. (1) and (2) of the previous section were found from the data of Scala et al, [5]. These investigators considered real gas effects and assumed dissociated equilibrium air behind a normal shock wave. The stagnation point conditions result from the isentropic compression of the gas behind the normal shock until the total or stagnation enthalpy value is reached. Thus,

$$H_o = H_2 + \frac{V_2^2}{2gJ} \tag{8}$$

and the stagnation temperature is a function of the total enthalpy and pressure,

$$T_o = f(H_o, P_o) \tag{9}$$

where

H_o = stagnation or total enthalpy, Btu/lb_m

H_2 = local or static enthalpy behind normal shock, Btu/lb_m

V_2 = speed of air behind normal shock, ft/sec

g = acceleration due to gravity, ft/sec^2

J = conversion factor from mechanical units of energy to thermal units, 778 ft-lb/Btu

T_o = stagnation or total temperature, °R

P_o = stagnation or total pressure, lb/ft^2

For the same speeds and altitudes an inspection of Scala's data on the temperatures behind a normal shock, T_2, indicates no discernible difference from the stagnation temperatures, T_o. The average velocity of the air components behind the normal shock is substantially subsonic, i.e., at a free stream Mach number of 18, the Mach number behind a normal shock is 0.32. Further, the speed term is squared and becomes negligible compared to the local or static enthalpy H_2. Therefore, the contribution of the term $V_2^2/2gJ$ to the total enthalpy H_o, and to the stagnation temperature T_o is insignificant. The highest temperature that the metal skin can reach, if radiation effects are not included, is the adiabatic wall or recovery temperature which can be found from the relations,

$$H_{aw} = H_2 + r_\alpha \frac{V_2^2}{2gJ} \tag{10}$$

and

$$T_{aw} = f(H_{aw}, P_{aw}) \tag{11}$$

where

H_{aw} = adiabatic wall enthalpy, Btu/lb_m
r_α = recovery factor, dimensionless
T_{aw} = adiabatic wall temperature, °R
P_{aw} = adiabatic wall pressure, lb/ft^2

It is seen by inspection of Eqs. (8) and (10) that the only difference between the stagnation enthalpy and the adiabatic wall enthalpy is in the recovery factor r_α in Eq. (10). However, since $V_2^2/2gJ$ is already very small, as discussed above, and since r_α is ≈ 0.85, the product $r_\alpha V_2^2/2gJ$ is also very small. Therefore, H_{aw} will approach (within 99.9 percent at M = 18), H_o. Therefore, T_{aw} will approach T_o and no numerical distinction can be made between the values of T_{aw} and T_o in the region of interest ($7<M_\infty<18$). These temperatures are shown in Figure 5.

Surface Temperature Determination

Procedure

By taking the stagnation temperature data of Figure 5, and assuming an emissivity for the metallic fabric of the spherical shells, it is possible to calculate the heat fluxes to the leading edges (stagnation surfaces). It is then possible to calculate the wall temperature at the leading edges. With the use of the approximate stagnation point heat transfer equation for laminar flow developed by Detra and Hidalgo, [16], one is able to find the convective heating as follows,

$$\dot{q}_s = \frac{865}{\sqrt{R}} \left(\frac{V}{10^4}\right)^{3.15} \cdot \sqrt{\frac{\rho_\infty}{\rho_{SL}}} \; \frac{H_o - H_w}{H_o - H_{w\ 300K}} \tag{12}$$

where,

$\dot{q}_s$ = Stagnation point heat transfer rate, $\frac{\text{Btu}}{\text{ft}^2\text{-sec}}$
R = Nose radius at stagnation point, ft
V = Instantaneous flight velocity, ft/sec
ρ_∞ = Instantaneous free stream atmsopheric density slugs/ft^3
ρ_{SL} = Atmospheric density at sea level, slugs/ft^3
H_o = Stagnation or total enthalpy, Btu/lb_m
H_w = Enthalpy of air at wall, Btu/lb_m
$H_{w\ 300K}$ = Enthalpy of air at wall at 300°K, Btu/lb_m

The convective heating is now added to the appropriate non-equilibrium radiation heating rate found from Figure A-9 and the total is set equal to the radiative cooling rate off the surface. Thus,

$$\dot{q}_s + \dot{q}_{n-e} = \dot{q}_r = \sigma\varepsilon T_w^4 \tag{13}$$

where,

σ = Stefan - Boltzman constant, $0.48\text{x}10^{-12}$ Btu/ft^2-sec-$^\circ$R^4

ε = Surface emissivity to space, dimensionless

T_w = Wall temperature, degrees Rankine

Figure 6 shows the surface temperatures found for the three spherical shells.

A sample calculation will now be made. The following conditions prevail for the 58.5 foot spherical shell at 329,000 feet altitude:

V = 21,600 ft/sec

R = 29.25 ft

$H_{w\ 300K}$ = 130 Btu/lb$_m$

$$\frac{\rho_\infty}{\rho_{SL}} = 0.33 \times 10^{-6}$$

$$\left.\begin{aligned} \frac{\rho_2}{\rho_{SL}} &= 1.35 \times 10^{-4} \\ T_o &= 8{,}300^\circ R \end{aligned}\right\} \quad H_o = 11{,}000 \text{ Btu/lb}_m$$

Assume T_w = 1350°R then H_w = 330 Btu/lb$_m$

Thus,

$$\dot{q}_s = \frac{1}{\sqrt{29.25}} \times 865 \left(\frac{21{,}600}{10^4}\right)^{3.15} \times\sqrt{0.33\text{x}10^{-6}}\ \frac{11{,}000-330}{11{,}000-130}$$

$$\dot{q}_s = 1.022 \text{ Btu/ft}^2\text{-sec}$$

(A computational check of $\dot{q}_s$ using the equilibrium air convection heating equation of Eggers, et al - [26], indicates $\dot{q}_s$=1.015 Btu/ft^2-sec.)

For the non-equilibrium air radiation to the surface it is found from Figure A-9 that for a velocity of 21,600 feet/second (6.59 km/sec) a heating rate of 2.03 Btu/ft^2-sec (2.3 watts/cm^2 will take place. Thus,

$\dot{q}_{n-e} = 2.03$ Btu/ft^2-sec

For the radiative cooling, we assume ε=0.5, (a value close to the total hemispherical emittance of a variety of alloys including rolled steel, Inconel, and stainless steel 304).

Then,

$$\dot{q}_r = (0.48 \times 10^{-12})\ (0.5)\ T_w{}^4$$

Now, setting $\dot{q}_s + \dot{q}_{n-e} = \dot{q}_r$ and solving for T_w we get,

$$1.022 + 2.03 = 0.24\ T_w{}^4 \times 10^{-12},$$

and,

$$T_w = 1888°R = 1428°F.$$

It is interesting to note that had the non-equilibrium radiation flux been neglected, the wall temperature for the 58.5 foot diameter sphere would have been 1440°R which is 448°R less than the temperature of 1888°R found above. For the 7 foot diameter sphere the maximum temperature neglecting non-equilibrium radiation would have been 3580°R which is only 80°R less than the temperature of 3640°R shown in Figure 6. (Previous to the year 1960, the magnitude of non-equilibrium radiation was unknown and therefore neglected in heat transfer calculations of reentering bodies. This is seen, for instance, in Hankey's work - page 53 of [17], and Chapman's work-Figure 16 of [25].)

For a further discussion of the heat fluxes to the leading edge, the reader is referred to Appendix B.

Determination of Deceleration

The analytical method of Chapman, [29] and [30], was used for calculating the deceleration during entry. The defining equation for the resultant deceleration is taken as

$$a \equiv \sqrt{\left(\frac{du}{dt} + \frac{uv}{r}\right)^2 + \left(\frac{dv}{dt} - \frac{u^2}{r} + g\right)^2} \qquad (14)$$

where,

a = resultant deceleration, ft/sec^2

g = gravitational acceleration of planet, ft/sec^2

t = time, sec

u = local horizontal component of velocity, ft/sec

v = local vertical component of velocity, ft/sec (positive if outward from planet center)

r = distance from planet center, ft

The basis of the analytical method is that the term uv/r can be neglected for atmosphere entry calculations. This simplification enables an analytic solution to the entry motion to be obtained.

Chapman shows in [30], that in order to reduce the pair of motion expressions for du/dt and dv/dt to a single equation, it is necessary to transform to a new dimensionless dependent variable Z. For the case of entry vehicles the equation that results for the deceleration is,

$$\frac{a}{g} = \frac{\sqrt{\beta r}\,\bar{u}\,Z}{\cos\,\theta}\sqrt{1 + \left(\tan\,\theta - \frac{L}{D}\right)^2} \tag{15}$$

where,

β = atmospheric density decay parameter, ft^{-1}, constant in planetary density vs. altitude relation

$\rho = \bar{\rho}_o\, e^{-\beta y}$ ($\bar{\rho}_o$ = 0.0027 slugs/ft^3; $1/\beta$=23,500 ft for earth)

$\bar{u} \equiv \frac{u}{\sqrt{gr}}$, ratio of local horizontal velocity to orbital velocity, dimensionless

$Z \equiv \frac{\bar{\rho}_o}{2\left(\frac{m}{C_D A}\right)}\sqrt{\frac{r}{\beta}}\,\bar{u}\,e^{-\beta y}$, dimensionless variable

m = mass of body, slugs

C_D= drag coefficient, dimensionless

A = entry vehicle reference area, ft^2

y = altitude, ft

θ = flight path angle relative to local horizontal direction; positive for climbing flight, negative for descent, degrees

L/D= lift to drag ratio

For nonlifting entry vehicles Eq. (15) becomes,

$$\frac{a}{g} = \frac{\sqrt{\beta r}\,\bar{u}\,Z}{\cos\,\theta}\sqrt{1 + (\tan\,\theta)^2} \tag{16}$$

Furthermore, $\sqrt{\beta r}$ for Earth entry is approximately 30, so that Eq. (15) can be further reduced to:

$$\frac{a}{g} = \frac{30\,\bar{u}\,Z}{\cos\,\theta}\sqrt{1 + (\tan\,\theta)^2} \tag{17}$$

Figure 7 presents the results for the resultant deceleration of nonlifting bodies as a function of velocity ratio.

From the viewpoint of human tolerance to acceleration stress, it is not only the peak deceleration which must be considered, but also the orientation of the body, the duration of stress, and the rate of onset of deceleration. Numerous experiments with centrifuges have shown that human tolerance is greatest in transverse orientation; that is, with either chest-to-back or back-to-chest loading (see, e.g., [31] or [32]). Centrifuge experiments also have shown that the magnitude of acceleration is relatively more important than the duration, in the sense that if the acceleration is increased 10 percent, the tolerable duration is decreased by a factor of about 2. Thus, a method believed to be conservative for calculating the effective duration Δt during entry is to assume that the maximum deceleration acts over the entire time it would take for this deceleration to slow the vehicle from orbital velocity to rest. A curve of maximum deceleration versus duration obtained in this manner from [30] is presented in Fig. (8) for various L/D ratios. Included in this figure is a boundary representing human tolerance in the transverse orientation for conditions of rapid onset of acceleration. This boundary also is conservative inasmuch as entry decelerations are built up relatively slowly under which conditions the body circulation builds up a reflex action of effectiveness. It is evident from both Figures (7) and (8) that the decelerations for orbital entry into the earth's atmosphere are within human tolerance. The human tolerance to deceleration after prolonged stay in weightlessness is at present thought to be less than the boundary level indicated in Figure 8. It appears to vary with individual astronauts and may depend on age. At present, the only experience gained in this area is that of the two week mission of the Gemini 7 crew in December of 1965. Neither astronaut of that mission was troubled or showed after effects by the deceleration upon reentry.

Loading of the Spherical Shells

The peak external loading of the spherical shells occurs when the inertia force due to the deceleration is at a maximum. The maximum fabric stress, on the other hand, occurs when the difference between internal and external pressure on the balloon is greatest. To maintain the balloon inflated, the pressure on the inside of the balloon must be greater than the dynamic pressure load balancing the inertia force. Since we are concerned here with manned rescue vehicles we would not want to take in ram air during the high velocity part of entry because the temperature of the air resulting from the conversion of the high kinetic energy of the ram air would be much too high for survival. Consequently, we would want to use a pressurized gas tank inside the balloon until we were below a certain speed at which time we would introduce ram air which would mix with the cooler gas (e.g., nitrogen, helium or air) already in the balloon.

As an example of the quantity of pressurized gas required and the magnitudes of the loads, we shall look at the conditions occuring at the point along the trajectories of maximum inertia force loading. This occurs at a velocity of 0.4 of orbital velocity for all spheres. At this point we have a stagnation total pressure (static plus dynamic) of $12.3\text{x}10^{-3}$ psia* for the 58.5 foot sphere. Therefore, pressurizing the balloon to about 2 times this value (since the Newtonian stagnation pressure is twice the free stream dynamic pressure) or 0.0246 psia, will keep the shell membrane in tension at all times.

To maintain an internal pressure greater than 0.0246 psia the following quantity of air is required:

$$V = \frac{4}{3} \Pi r^3$$

$$V = \frac{4}{3} \Pi (29.25)^3 = 104{,}800 \text{ ft}^3$$

and from the perfect gas law,

$$W = \frac{\rho V}{RT}$$

$$W = \frac{24.6\text{x}10^{-3} \text{ x } 144 \text{ x } 104{,}800}{53.3 \text{ x } 600} = 13.1 \text{ lbs.}$$

where,

ρ = Pressure, psf

V = Volume, ft^3

R = Gas constant, 53.3 $\text{ft-lb}_f/\text{lb}_m{}^\circ\text{R}$

T = Temperature, degrees Rankine, assumed 600°R

For the 7 foot sphere, the stagnation pressure will be $6\text{x}10^{-2}$ x 14.7 = 0.882 psia. Therefore, pressurizing the sphere above the Newtonian stagnation pressure of 2x0.882= 1.764 psia will keep the shell membrane in tension at all times.

To maintain an internal pressure greater than 1.764 psia the following quantity of air is required,

$$V = \frac{4}{3} \Pi r^3$$

---

*This value is obtained from Figure 9 of [5].

$$V = \frac{4}{3} \pi (3.5)^3$$

$$V = 179.8 \text{ ft}^3$$

and from the perfect gas law,

$$W = \frac{\rho V}{RT}$$

$$W = \frac{1.764 \times 144 \times 179.8}{53.3 \times 600}$$

$$W = 1.425 \text{ lbs.}$$

It is thus seen that only a minimal amount of gas is needed inside the spheres in order to maintain them inflated during reentry. However, due to pressure variations along the spherical surface (in hypersonic flow, these pressures can be approximated by the Newtonian distribution $p = p_{stag} \times \text{cosine}^2 \theta$ plus ambient on the front surface and by ambient on the trailing surface), surface deformations will result to the extent that the sphere material is elastic. If these are significant, they in turn could affect the surface temperatures resulting from drag and nose radius variations. Local stiffening would reduce these effects but might detract from the advantages of a simple spherical shape.

Weight Limitations

In the present work 680 pound spheres were considered. The assumption was made that the shell itself would weigh 250 pounds and that the astronaut, support devices, life support, insulation, retrorocket and all other equipment would weigh the remaining 430 pounds. For the case of steel shells the skin weight results in a skin thickness of 5.56×10^{-4} inches for the 58.5 foot diameter spherical shell. It is doubtful that a metallic fabric with a sealing film and an insulation layer could be made within this thickness limitation. Also, such a thin skin could easily tear while the astronaut is donning the device. It is felt that a minimum practical skin thickness is approximately 5 thousandths of an inch.* A 20 foot diameter steel spherical shell would have a thickness of,

---

*Reference [37] suggests use of a nickel-chromium alloy for use in an expendable disk module. The alloy metal fabric is woven from a yarn made of fine filaments (0.0005 inch) and resembles a lightweight canvas. This is impregnated with a resin compound which provides impermeability and a degree of rigidization. The total thickness of this material is 0.015 inch.

$$\rho \times A \times h = W$$

$$(1728 \times 0.29) \times 4\pi (10)^2 \times h = 250$$

$$h = 0.397 \times 10^{-3} \text{ ft or } 0.00476 \text{ in}$$

Therefore, because of the weight limitation, a spherical shell larger than 20 feet in diameter is not feasible as a rescue device.

2033-JJ-dfr

J. Jellinek

J. Jellinek

Attachments
- Figures 1-10B
- References
- Appendix A
- Appendix B

REFERENCES

1. Briefing - Space Rescue, Aerospace Corporation, Contract No. AF 04 (695)-66, (Confidential) prepared for Commander Space Systems Division, Air Force Systems Command, Los Angeles Air Force Station, Los Angeles, California 11 Feb 66 - Chart 49, Goodyear proposal (Unclassified).

2. Loh, W.H.T., "A Second-Order Theory of Entry Mechanics Into a Planetary Atmosphere," J. Aerospace Sci. 29, 1210-1221, 1237 (1962).

3. U. S. Standard Atmosphere, 1962, prepared under sponsorship of NASA, USAF and USWB.

4. Tsien, Hsue-Shen, "Superaerodynamics, Mechanics of Rarefied Gases," Journal of the Aeronautical Sciences, Vol. 13, December 1946, pages 653-664.

5. Scala, S.M., Gilbert, L.M. Cook, C.A., "Normal Shock Wave Calculations in Air at Flight Speeds up to 25,000 ft/sec," Technical Information Series Report No. R 62SD76, Space Science Laboratory, General Electric, Missile and Space Division, Philadelphia, Pa., November 1962.

6. Yoshikawa, K. K., and Chapman, D. R., "Radiative Heat Transfer and Absorption Behind a Hypersonic Normal Shock Wave", Ames Research Center Moffett Field, Calif., NASA Technical Note D-1424, September 1962.

7. Keck, J. C., Camm, J. C., Kivel, B., and Wentink, Jr., T., "Radiation from Hot Air. Part II. Shock Tube Study of Absolute Intensities", Annals of Physics: Vol. 7, 1959, pp. 1-38.

8. Wentink, T. Jr., Planet, W., Hammerling, P. and Kivel, B. "Infrared Continuum Radiation from High Temperature Air", J. Appl. Phys., April 1958, pp. 742 - 743.

9. Treanor, C. E., "Radiation at Hypersonic Speeds", Hypersonic Flow Research, ed. by Frederick R. Riddell, Progress in Astronautics & Rocketry - Vol. 7, pp. 255 - 280.

10. Page, W. A., and Arnold, J. D., "Shock-Layer Radiation of Blunt Bodies at Reentry Velocities", Ames Research Center, Moffett Field, Calif., NASA Technical Report R-193, April 1964.

11. NASA SP-55 (Air Force ML-TDR-64-159) papers entitled "Theoretical and Experimental Studies of the Total Emittance of Metals" by W. J. Parker and G. L. Abbott , "Surface Properties

of Metals" by H. H. Blau, Jr., and H. A. Francis, and "Method and Equipment for Measuring Thermal Emittance of Ceramic Oxides from 1200° to 1800°K, by H. E. Clark and D. G. Moore. Symposium on Thermal Radiation of Solids, San Francisco, California, March 4-5-6, 1964.

12. Camm, J. C., Kivel, B., Taylor, R. L., and Teare, J. D., "Absolute Intensity of Non-Equilibrium Radiation in Air and Stagnation Heating at High Altitudes", AVCO-Everett Research Laboratory, Everett, Massachusetts, Research Report 93, December 1959.

13. Goulard, R., "Radiation Transfer Regimes in Hypersonic Flight", Supersonic Flow Chemical Processess and Radiative Transfer, ed. by D. B. Olfe, and V. Zakkay, AGARD-NATO presentation, Pergamon Press, 1964, pp. 307-318.

14. Kivel, B., "Radiation from Hot Air and Its Effect on Stag-nation - Point Heating", Journal of the Aerospace Sciences, February, 1961, pp. 96-102.

15. Teare, J. D., Georgiev, S., Allen, R. A., "Radiation from the Non-equilibrium Shock Front", Hypersonic Flow Research, ed. by Frederick R. Riddell, Progress in Astronautics and Rocketry - Vol. 7, pp. 281-317.

16. Detra, R. W., and Hidalgo, H., "Generalized Heat Transfer Formulas and Graphs for Nose Cone Reentry Into the Atmosphere", Am Rocket Society, March 1961, pp. 318-321.

17. Hankey, W. L. Jr., Neumann, R. D., and Flinn, E. H., "Design Procedures for Computing Aerodynamic Heating at Hypersonic Speeds, Wright Air Development Division, USAF, Wright-Patterson Air Force Base, Ohio, WADC Technical Report 59-610, June 1960, Figure 12, p. 86.

18. Fay, J. A., and Riddell, F. R., "Theory of Stagnation Point Heat Transfer in Dissociated Air," Journal of the Aeronautical Sciences, Vol. 25, No. 2, February 1958, pp. 73-85.

19. Feldman, S., "Hypersonic Gas Dynamics Charts for Equilibrium Air", AVCO-Everrett Research Lab., Everett, Mass., Jan. 1957.

20. Rosner, D. E., "Scale Effects and Correlations in Nonequilibrium Convective Heat Transfer," Am. Inst. of Aeron. and Astron., Vol. 7, No. 7, July 1963, pp. 1554.

21. Goulard, R., "On Catalytic Recombination Rates in Hypersonic Stagnation Heat Transfer," Jet Propulsion Laboratory, November 1958, pp. 737-745.

22. Hansen, F. C., "Approximations for the Thermodynamic and Transport Properties of High-Temperature Air," NASA Technical Report R-50, 1959.

23. Scala, S. M., and Gilbert, L. M., "Theory of Hypersonic Laminar Stagnation Region Heat Transfer in Dissociating Gases," General Electric Missile and Space Division, Technical Information Series R 63SD40, Table II, p. 36.

24. Meyerott, R. E., "Radiation Heat Transfer to Hypersonic Vehicles", LMSD-2264, 8 Nov 1957, Lockheed Aircraft Corp., Palo Alto, Calif.

25. Chapman, D. R., "An Approximate Analytical Method for Studying Entry into Planetary Atmospheres," NACA Technical Note 4276, Ames Aeronautical Laboratory, Moffett Field, Calif., May 1958.

26. Eggers, A. J., Jr., Hansen, F. C., and Cunningham, B. E., "Stagnation-Point Heat Transfer to Blunt Shapes in Hypersonic Flight, Including Effects of Yaw", NACA Technical Note 4229, Washington, April 1958.

27. Meyerott, R. E., Sokoloff, J., and Nicholls, R. W., "Absorption Coefficients of Air", Geophys. Res. Paper 68, July 1960. (Also LMSD 288052, Lockheed Aircraft Corp., 1959)

28. Kivel, B., and Bailey, K., "Tables of Radiation from High Temperature Air", Avco Res. Rep. 21, 1957.

29. Chapman, D. R., "Deceleration During Entry into Planetary Atmospheres," Physics and Medicine of the Atmosphere and Space, New York - London, John Wiley & Sons, Inc., 1960, pp. 339-351.

30. Chapman, D. R., "An Approximate Analytical Method for Studying Entry Into Planetary Atmospheres", NACA Technical Note 4276, Ames Aeronautical Laboratory, Moffett Field, California, May 1958.

31. Dempsey, C. A., "Human Protection in Abrupt Acceleration Environments", Institute of Environmental Sciences, 1961 Proceedings, pp. 365-369.

32. Stapp, J. P., "Effects of Linear Acceleration", Aerospace Medicine, ed. by Maj. Gen. Harry G. Armstrong, USAF (Ret.), Baltimore 1961, The Williams & Wilkins Company, pp. 268-269.

33. Allen, R. A., Rose, P. H., and Camm, J. C., "Nonequilibrium and Equilibrium Radiation at Super-Satellite Reentry Velocities", IAS 63-77, IAS 31st Annual Meeting, January 1963.

34. Canning, Thomas N., and Page, William A., "Measurements of Radiation From the Flow Fields of Bodies Flying at Speeds up to 13.4 Kilometers per Second". Paper presented to the Fluid Mechanics Panel of AGARD, Brussels, Belgium, April 1962.

35. Clark, Howard E., Moore, Dwight G., "Method and Equipment for Measuring Thermal Emittance of Ceramic Oxides from 1200° to 1800°K, "Symposium on Thermal Radiation of Solids, edited by S. Katzoff, NASA, held at San Francisco, California, March 4-6, 1964.

36. NASA SP-55 (Air Force ML-TDR-64-159), Surface Properties of Metals", by H. H. Blau, Jr. and H. A. Francis, Symposium on Thermal Radiation of Solids, San Francisco, California, March 4-6, 1964.

37. Mavriplis, F., "Reentry Crew Escape Module Concepts for Orbital Vehicles", 5th Congress of the International Council of the Aeronautical Sciences, London, England, September 12-16, 1966. (ICAS Paper No. 66-35)

38. Ross, J. H., "Flexible Fibrous Materials and Coatings for Expandable Reentry Systems", Aerospace Expandable Structures Conference Transactions, Air Force Aero Propulsions and Air Force Flight Dynamics Laboratories, Dayton, Ohio, October 23-25, 1963, p. 74.

SYM	SOURCE	TYPE	M_∞	H_W
○	LDH TUNNEL	FREE-FLIGHT	≃ 11	-0.92
●	"	"	"	-0.91
△	"	"	"	-0.88
▽	"	"	"	-0.85
□	"	BALANCE	≃ 10	-0.74
×	VKF TUN C	"	"	-0.32

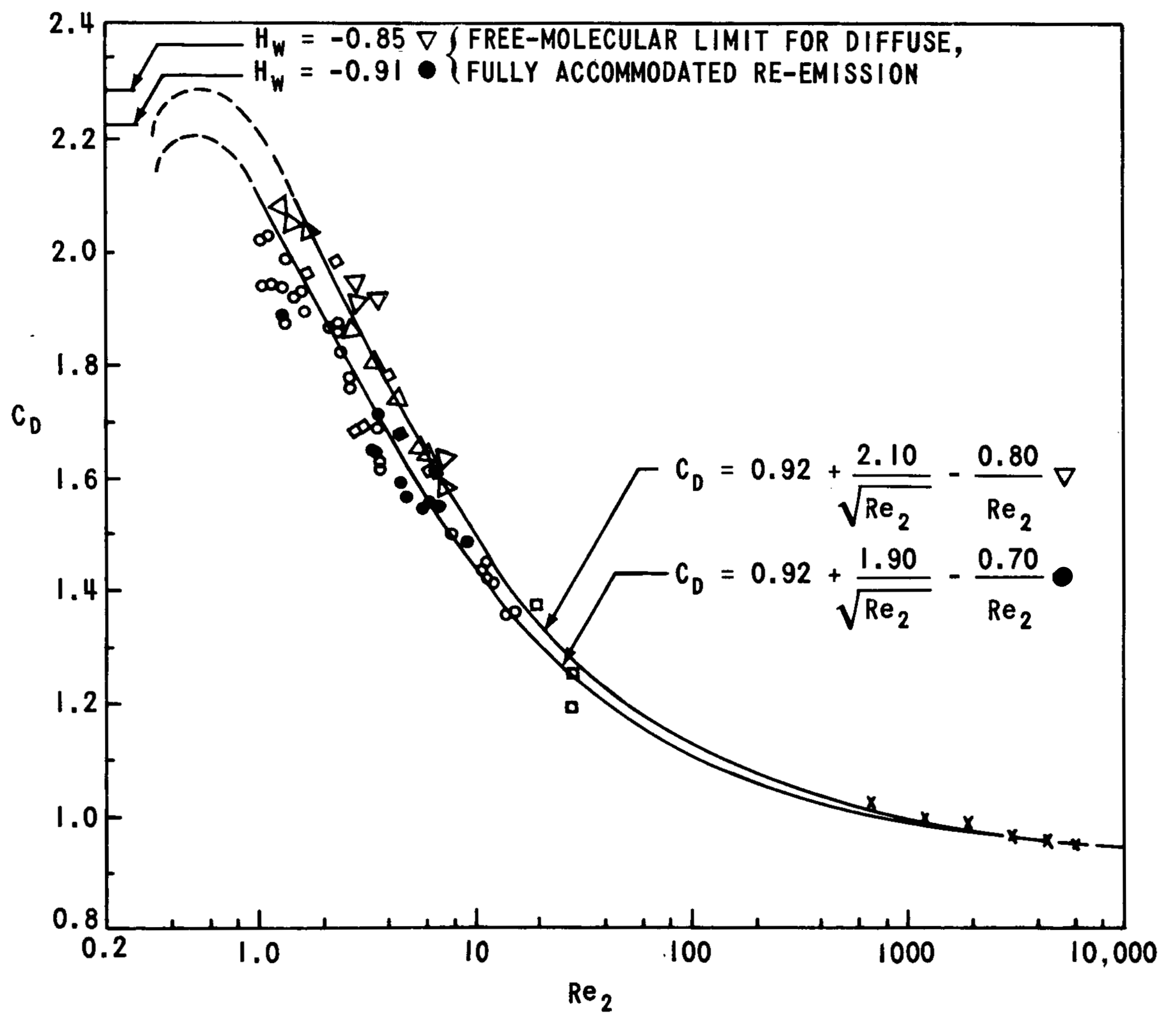

FIGURE 1 - DRAG OF SPHERES IN HYPERSONIC FLOW WITH $H_W < H_0$: NEW DATA. REFERENCE 7

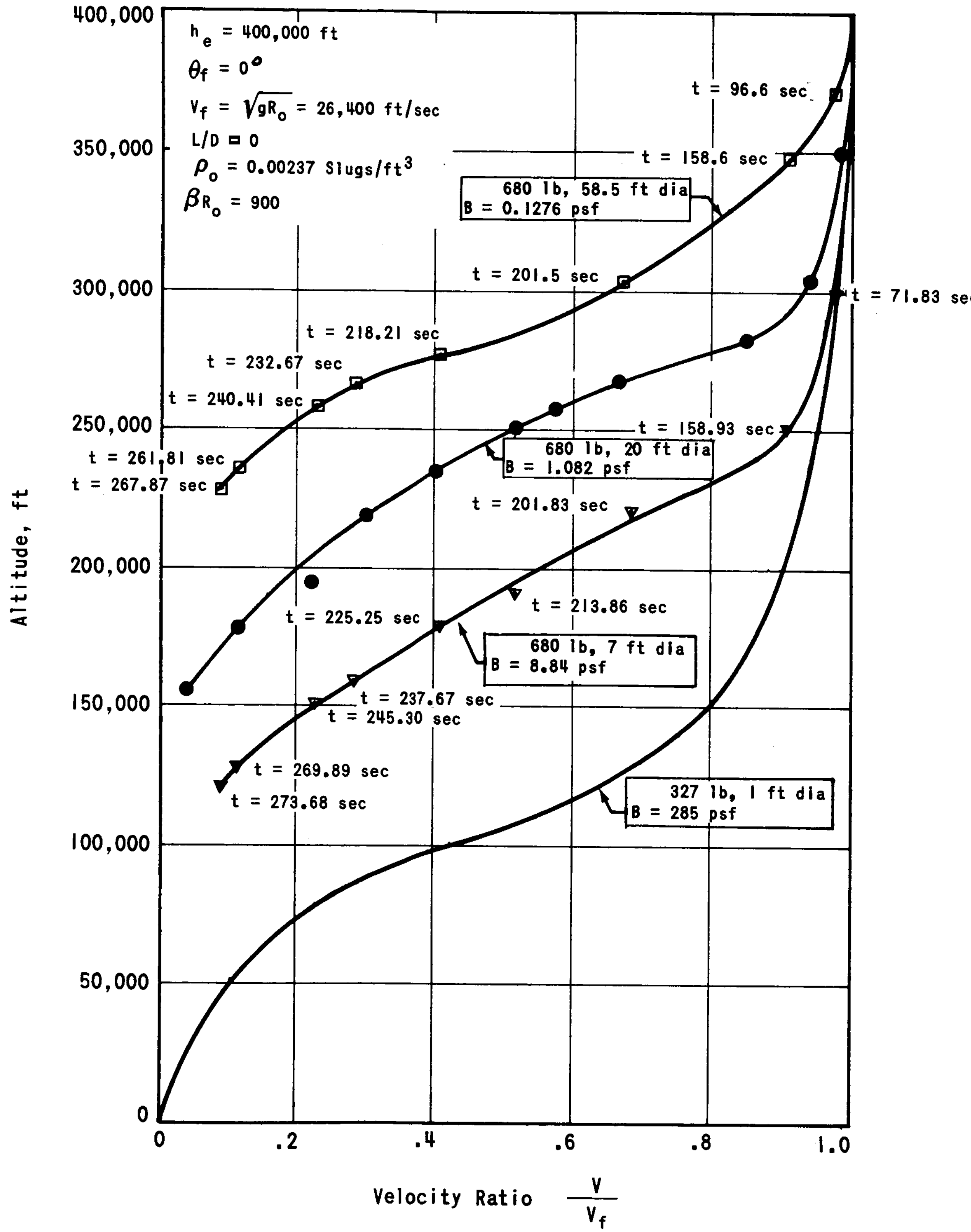

FIGURE 2 - TRAJECTORY PROFILES FOR SPHERES ENTERING TANGENTIALLY FROM CIRCULAR ORBIT

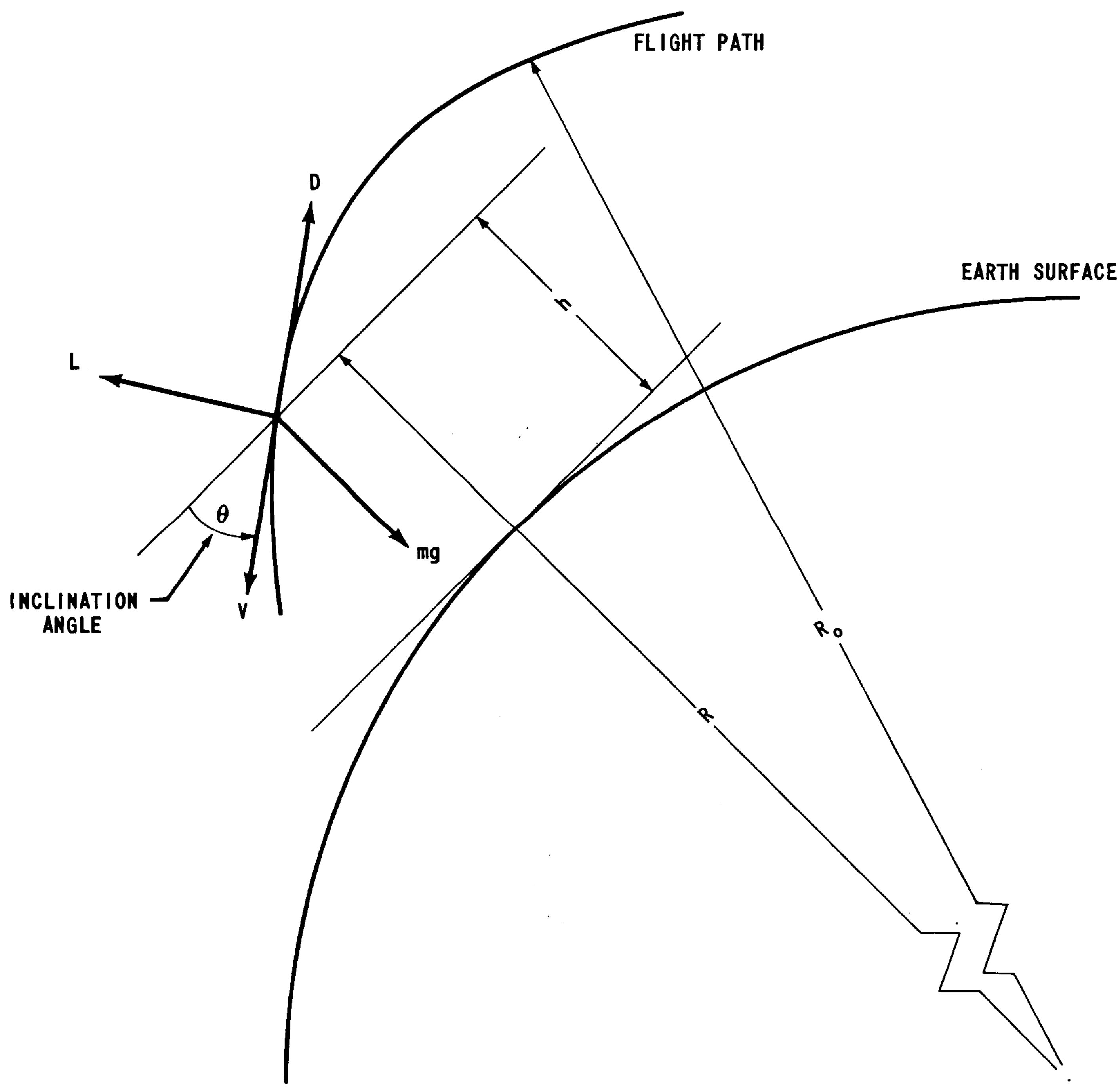

FIGURE 3 - ENTRY GEOMETRY AND NOMENCLATURE

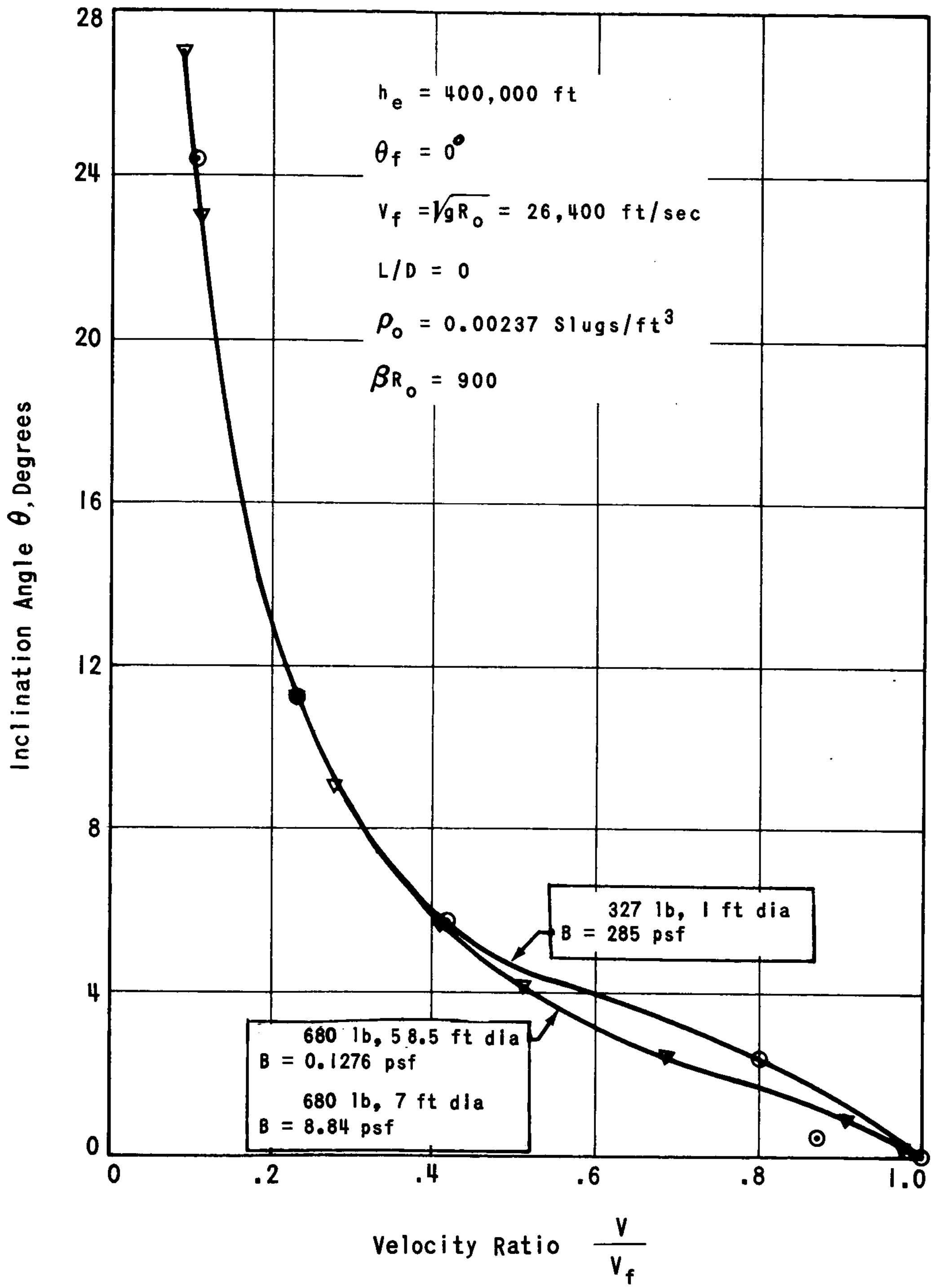

FIGURE 4 - INCLINATION ANGLES FOR SPHERES DURING ENTRY FROM CIRCULAR ORBIT

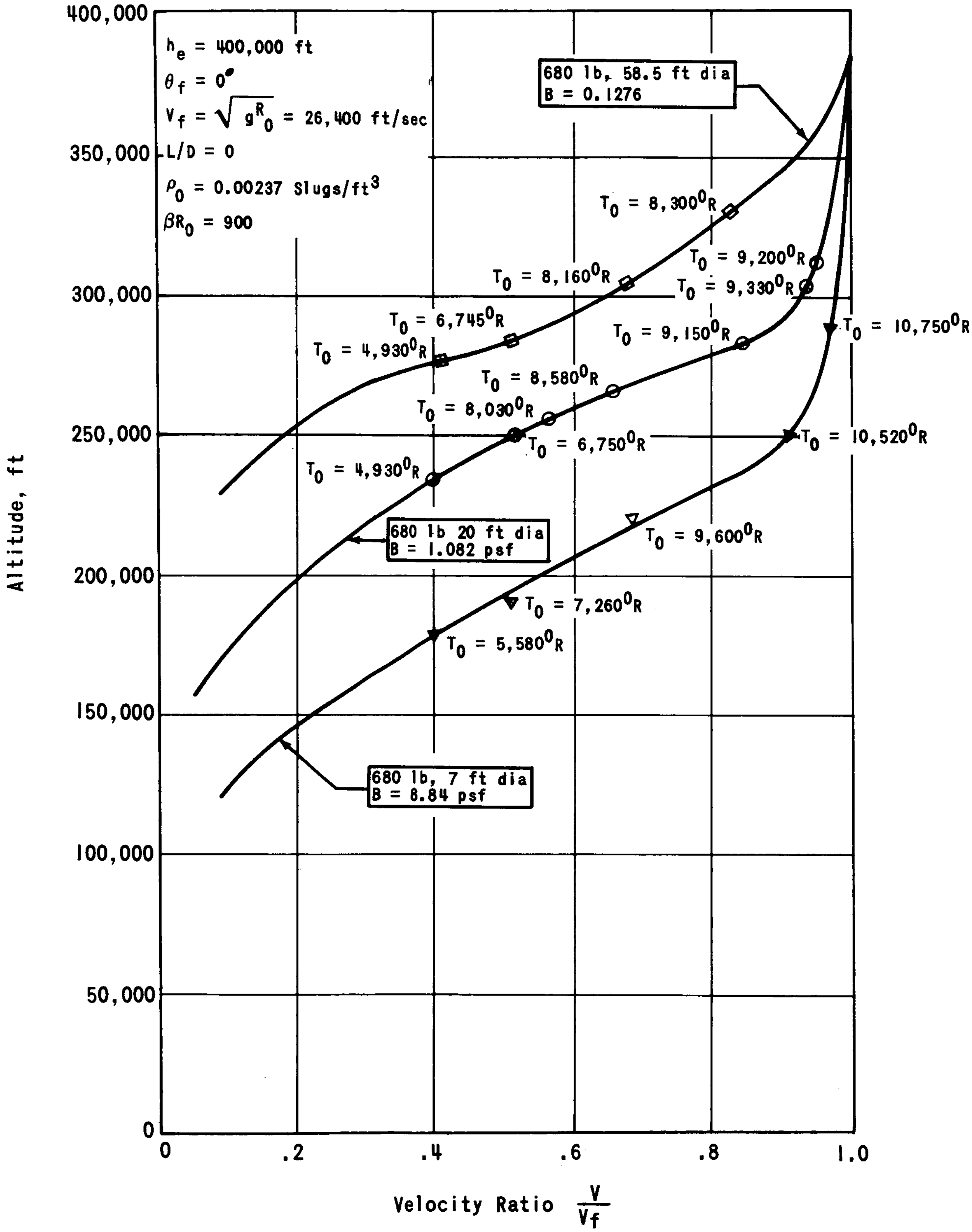

FIGURE 5 - STAGNATION TEMPERATURES FOR SPHERES ENTERING TANGENTIALLY FROM CIRCULAR ORBIT

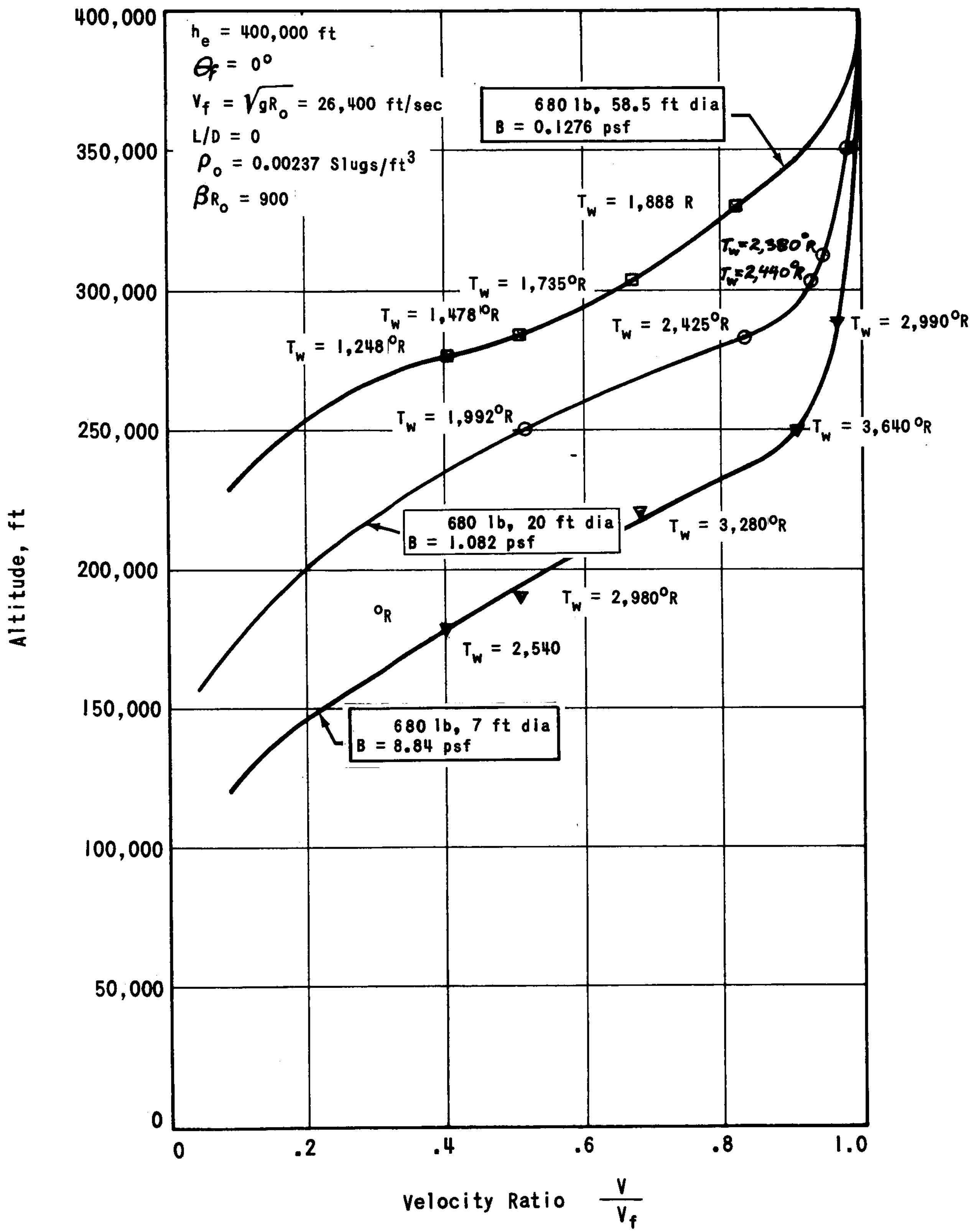

FIGURE 6 - LEADING EDGE WALL TEMPERATURES FOR SPHERICAL SHELLS ENTERING TANGENTIALLY FROM CIRCULAR ORBIT

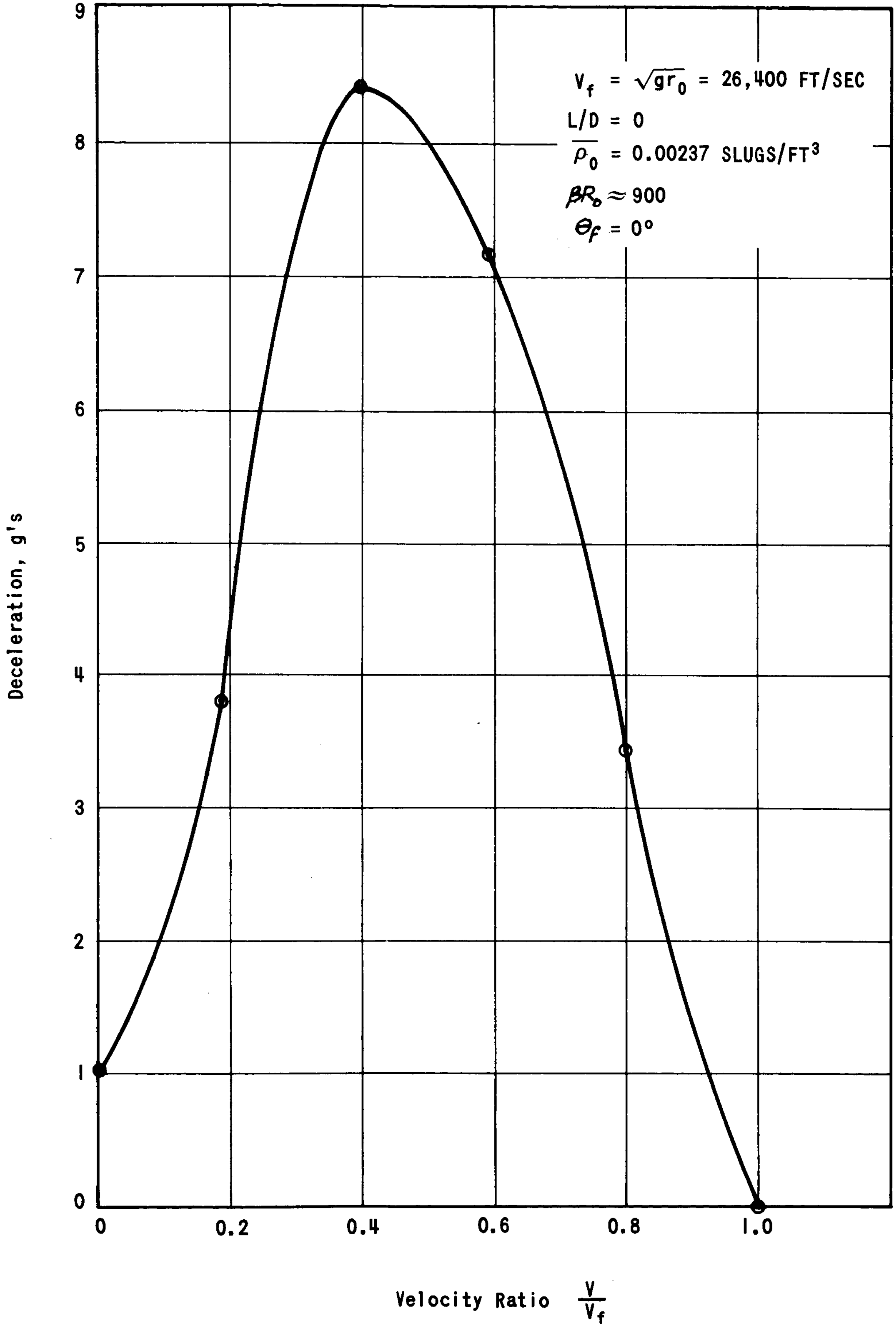

FIGURE 7 - DECELERATION OF SPHERES ENTERING EARTH'S ATMOSPHERE AT SHALLOW ANGLE

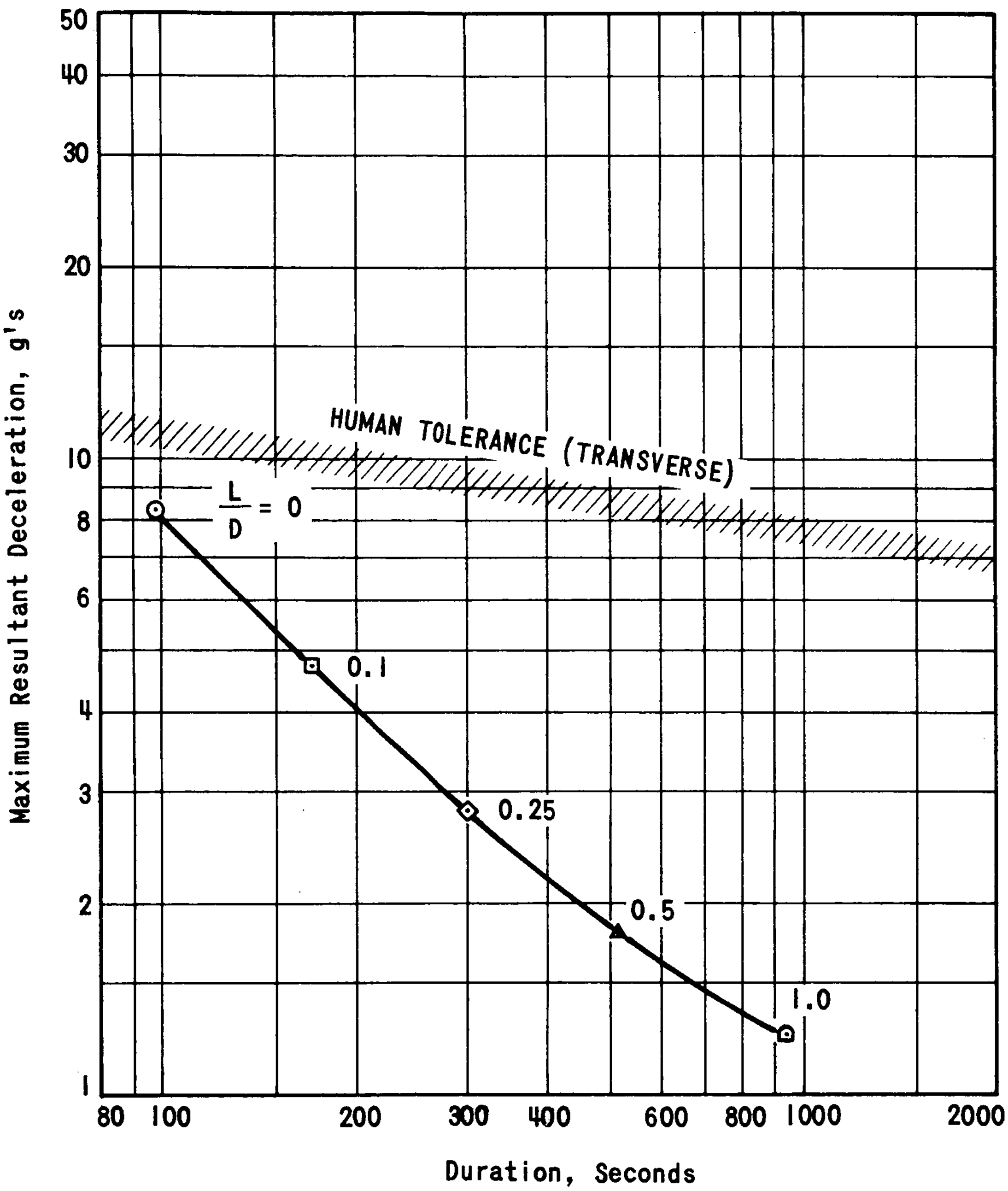

FIGURE 8 - LEVEL AND DURATION OF DECELERATION FOR ENTRY INTO THE EARTH'S ATMOSPHERE FROM DECAYING ORBITS

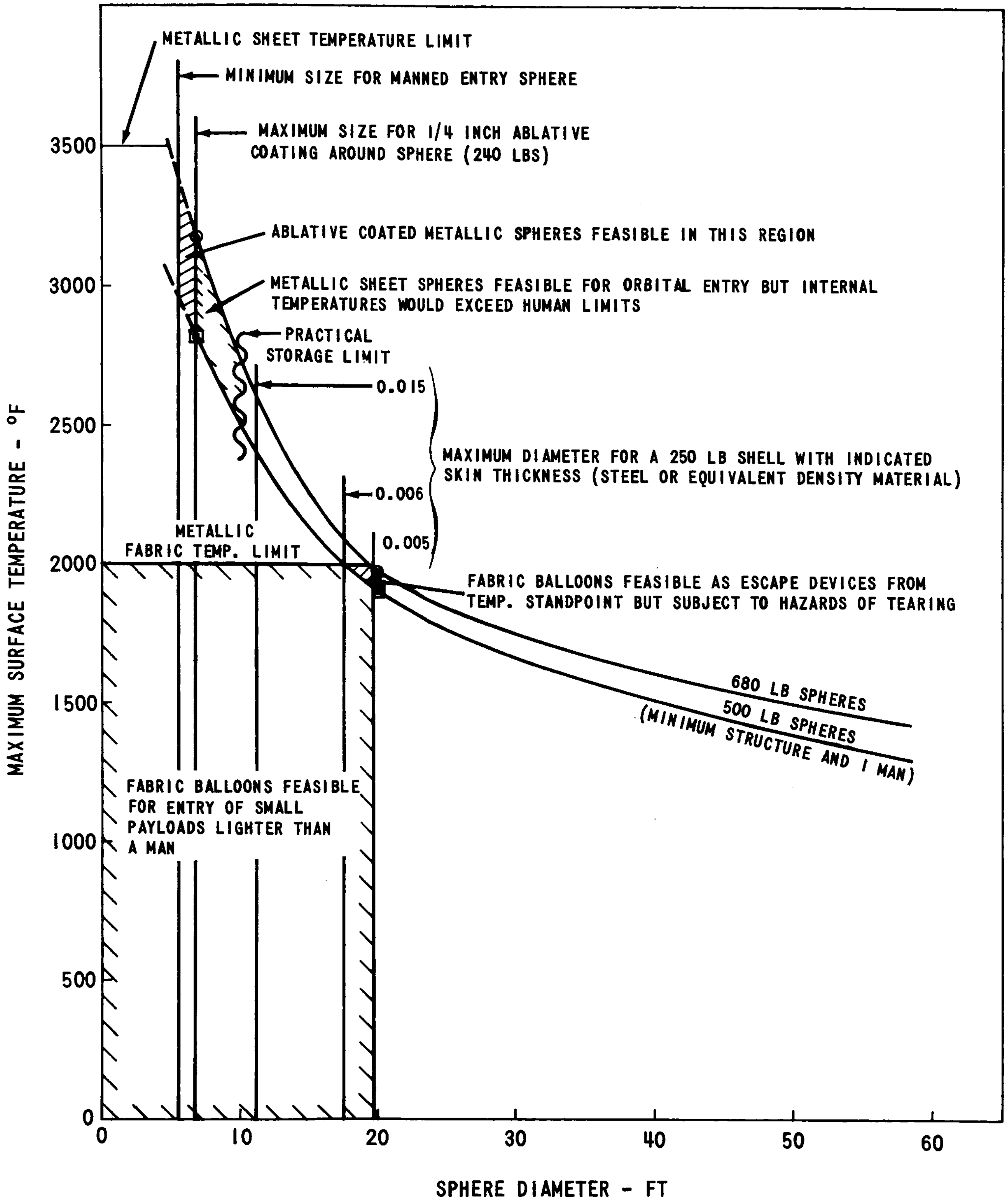

FIGURE 9 MAXIMUM SURFACE TEMPERATURES VS. SPHERE DIAMETER FOR 500 LB AND 680 LB SPHERES SHOWING REGIONS OF PRACTICAL APPLICATION TO ORBITAL ENTRY DEVICES

APPENDIX A - REVIEW OF LITERATURE ON HIGH TEMPERATURE AIR RADIATION AND RADIATION COOLING FROM THE SURFACE OF ENTERING BODIES

Wavelengths of Air Radiation and Wavelengths of Metal Surface Radiation

Computations of the radiant energy transported to an entering body were made assuming an adiabatic, nonabsorbing media. This assumption is approximately satisfied when the heating rate is small compared to black body radiation ($q<<\sigma T^4$) and when the radiant heating rate is small in comparison to the freestream kinetic energy rate [$q<<(1/2J)\ \infty V^3_\infty$]. Both of these conditions place an upper limit on the energy that can be radiated to an entry vehicle per unit time. When q is of the order of σT^4, significant gas self-absorption of radiation occurs. Conversely, when q is of the order of $(1/2J)\ \infty V^3_\infty$), "decay" of the flow energy occurs; i.e., a significant portion of the total flow energy is dissipated as radiant energy.

Results of Yoshikawa and Chapman [6] shown in Figure A-1, illustrate the flow regimes for a gray gas. Also shown are the trajectory lines for bodies having an L/D=0 and ballistic coefficient W/C_DA of 0.1276 psf, and W/C_DA=8.84 psf along with shock standoff distance regimes of 0.1 ft, 1.0 ft and 10 ft. For the 58.5 ft sphere at 329,000 feet altitude the velocity is 21,600 feet/second, and the shock standoff distance is calculated to be 1.75 feet*. For the 7 ft sphere at 250,000 feet, the velocity is 24,300 feet per second, and the shock standoff distance is calculated to be 0.173 feet. Figure A-1 indicates that the flow fields for manned entry from near-Earth orbits lie outside both the absorption and the decay flight regimes and therefore the effects of gaseous self-absorption and decay are not of importance.

While in principle the radiation by atoms and molecules is completely predictable from known quantum mechanics laws, in practice the theory must usually be augmented by experiment to obtain absolute intensities. This was a central aim of Keck et al, [7]. For the case of molecules, which are the most intense source of radiation from air, it involves determination of the electronic transition probabilities or f-numbers. The development of the shock tube has made possible the quantitative study of both the emission and absorption of radiation in gases at high temperatures.

---

*The standoff distance δ, depends upon the radius of curvature R of the nose and ρ_1/ρ_2, the air density ratio across the shock. It has been shown i.e. see Reference [24] to be approximately $\delta \simeq R\rho_1/\rho_2$.

Under appropriate conditions it is possible to produce a uniform sample of gas in thermodynamic equilibrium at accurately known temperature and pressure. The obvious disadvantage of the shock tube is that the conditions are transient, lasting only from 10 to 100 micro-seconds. However, modern techniques in electronics and spectroscopy make it possible to obtain much valuable data even in this short time interval. The intensity of the radiation from air (21% O_2+79% N_2 at a density of 0.83 atmospheres) heated by reflected shock waves is shown as a function of wavelength from 0.2 to 1.0 microns in Figure A-2. The curves were constructed by [7] from theory given in his text. Figure A-3 taken from Wentink et al, [8], shows experimental absolute radiation intensities along with two calculated curves for air at higher wavelengths - the infrared region. Experimental data was also obtained by reflecting plane shocks in a shock tube. Treanor, [9], reviewed the available data for radiation from equilibrated high temperature air. He presented the available results in graphical form, showing the absorption coefficient for each radiating species as a function of temperature and wavelength. The temperature range considered was from 3000°K, to 8000°K, the wavelength range was from 0.2 to 1.5 microns. Seven molecular band systems were considered. For two of these (NCγ and O_2S-R) there was good agreement among the various experimental results. For four bands (N_2 (1+), N_2^+ (1-), NOβ and NO_2 continuum) there was substantial disagreement. For the other molecular band system (N_2 (2+)), and for the oxygen free-bound and free-free radiation, there was only a single source of data.

The process of developing theoretical predictions of thermal radiation from air in thermochemical equilibrium consists of calculating the radiation intensity from a unit amount of each species present, and then, with knowledge of the equilibrium composition of the air, adding up the various contributions to obtain the total radiation. The determination of the radiative intensity as a function of temperature from a particular species is mathematically difficult and has led to various simplifications and, in most cases, to the necessity of determining experimentally an unknown parameter in the equation for the intensity. For example, the radiative intensity from a single excited electronic state of a molecule can be expressed as

$$E \sim P\, n h \nu \qquad \text{(A-1)}$$

where E is the radiative intensity, P is the transition probability (Einstein A coefficient) of an electronic transition, n is the number of molecules in the excited electronic state, h is Planck's constant, and ν is the frequency of the resultant radiation (see, e.g., [10]). The transition probability, in turn, may be approximated by

$$P \sim (h\nu)^2\, f_e f_v f_r \qquad \text{(A-2)}$$

where P has now been factored into three components related to the electronic, vibrational, and rotational excitation of the molecule. All but one of the components of the probability function can be computed from reasonable models of the molecular structure by use of wave mechanics. Usable values of the remaining transition probability, the electronic f number, have thus far only been determined from experiment. A multiplicity of such expressions must be summed, usually with simplification as to the wavelength structure of the radiation, to obtain an estimate of the total radiation from a given molecular species. Radiation caused by the interaction of free electrons with neutral or ionized particles (so-called free-free or free-bound sources) is normally approximated with the classical Kramer's formula (c.f.) [7]. The adjustable parameter here is the effective charge Z of the particle involved in the interaction. Again, Z can be adjusted to fit experiment to theory. The available predictions for equilibrium air radiation are therefore, in a sense, hybrid in that they consist of a mixture of theory and experiment.

It should be noted that the species causing the predominant radiation varies with temperature. For example, at temperatures of 5000° to 7000°K, the NOβ and NOγ molecular bands have large contributions; at temperatures of 7000° to 9000°K, the N_2+ (1-) molecular band is important; whereas increasing ionization at temperatures above 10,000°K causes free-free and free-bound radiation from the neutral and ionized atoms of N and O to have a large contribution to the total radiation.

Presented in Figure A-4 are low resolution spectra from [10] provided by narrow-band radiometers consisting of photomultiplier and narrow-band optical filter combinations. The instruments viewed the model at right angles to the flight path through narrow slit assemblies. The models were launched by light-gas guns into still air into a countercurrent air stream generated by a shock-tube-driven hypersonic wind tunnel. The spectra were selected to show the effect of density at velocities near 20,000 feet/sec. The additional spectrum at 33,500 feet/sec. is included to show velocity effects. Included on the figures are theoretical predictions for the observed radiation, W_λ, obtained from the equilibrium air radiation calculations of Meyerott et al [27], and Kivel and Bailey [28]. Basically, the equilibrium prediction for W_λ is obtained by calculating the equilibrium thermodynamic values of temperature and density in the bow-shock region, assigning values of radiative intensity to each volume element, and then integrating over the volume in the field of view of the radiometer. The theoretical predictions of W_λ compare favorably, from the standpoint of both spectral shape and intensity, with the experimental spectra in the ultraviolet (0.2 to 0.5 micron) region at the higher density, Figure A-4a. The comparison degrades at 20,000 ft/sec as the density is lowered. The reason for the low-estimate for radiation at low densities given by the equilibrium theory has been recognized [10] as due to the appearance of predominant nonequilibrium regions in the shock layer of the model and consequent increase of radiative intensity.

Figure A-5 shows the spectral emittance for polished platinum that had been annealed for 1 hour in air at 1525°K. Changes in the chemical nature of a surface can significantly alter emittance or reflectance properties essentially by altering the emitting or reflecting material. Such effects are most significant at high temperatures, where reaction rates are large, but can be important at low temperatures as well. Oxidation reactions are most frequently encountered. Figure A-6 rather dramatically illustrates the effects of surface oxidation on stainless steel. It is a graph of spectral emittance for stainless steel as a function of wavelength from 2 to 14μ. The lower curve is for a sample heated in air for 3 hours at 600°C, and the upper curve is for a sample heated in air for 6 hours at 1000°C. The actual state of the metal near the surface (e.g., the identity, the density of the absorbed impurities, the surface irregularities) are generally not known, and one does not know what to use for the electron wave functions near the surface. These are crucial for any theory of emissivity of metals since only the electrons that are near the surface absorb or emit radiation. In addition one finds that the published literature on emissivity is based on considerations of thermal equilibrium between a solid and its environment, whereas during reentry, the surface of the vehicle is exposed to a changing thermal environment.

Precise emittance values can, however, be obtained from reflectance measurements while in thermal equilibrium, with an uncertainty in the best cases of as little as ±0.001. In Figures A-5 and A-6 it is seen that all of the energy of radiative emission is in the infrared region, i.e., at wavelengths greater than 1 micron. It is seen by comparing the air radiation data of Figures A-3 and A-4 with the emission data of platinum and oxidized stainless steel - Figures A-5 and A-6, that the air radiates very little to the surface above 0.5 microns at entry velocities up to 33,500 feet/second and conversely the hot air is mostly transparent to the radiation emitted by the metals.

Equilibrium Radiation of Air

Figure A-7 taken from Kivel [14], is a plot of the radiation energy per unit volume. To convert from the total energy radiated to the energy radiated toward the body it is necessary to divide by 2 because half of the radiation leaves each side from a thin slab of radiating gas. In order to make estimates of radiative heat transfer from equilibrium air, it is necessary to locate the flight trajectory on the altitude velocity map of Figure A-7 and to multiply the energy radiated per unit volume by the detachment distance in cm.

As can be seen from Figure A-7, the radiation heating of an entry body increases rapidly with increasing flight velocity and decreasing altitude. A body that reenters at high speed and high drag avoids the high radiation region because it decelerates at high altitudes. This is seen by the trajectories of the two spherical shells of Figure 5 which are superimposed on Figure A-7.

The equilibrium predictions of radiation intensity given in Figure A-7 are subject to several limitations. Some of these limitations, which are important at higher altitudes are delineated in Figure A-8. At very high altitudes a shock wave is not formed in front of the entering vehicle. (This a conditions that was described previously as free molecular flow.) The equilibrium radiation predictions do not hold for this regime any more than do the convection predictions in the free molecular regime.

We next come to the transition region in which a detached shock forms in front of the vehicle. In this region the surface will have a strong cooling effect on the gas behind the shock. At a somewhat lower altitude the viscous part of the shock layer is sufficiently thin so that there is a high-temperature inviscid region. This is the beginning of the gas-dynamics continuum region. The limiting line, labelled "continum flow" is based on a Knudsen number $K=\lambda/R = 0.01$.

The next correction to be considered is the diminution of radiation because the radiation-producing collisions are too infrequent compared to the rate of emitted radiation. This phenomena is called collision limiting, and depends primarily on the gas density. It also depends on the time for molecular radiation, which varies from 10^{-6} to 10^{-8} seconds for air components. When the density is sufficiently high there are sufficient collisions to maintain the excited state population in equilibrium with the ground state. Only a small proportion of the excited molecules are de-excited by emission of a photon. At lower densities, however, the number of collisions in a unit time becomes comparable with the rate of radiative de-excitation. The excited state population then falls below the local equilibrium level which prevailed at high density. An analogy may be drawn by consideration of the filling of a pail which has a hole in it. If a sufficient flow of water is directed into the pail, the water in the pail will reach a certain equilibrium level. If the flow into the pail is reduced, then this equilibrium level will be lowered. A mean height for the onset of collision limiting is indicated in Figure A-8 by the "collision limited" line drawn by assuming a mean radiation lifetime of 10^{-7} seconds and a de-excitation collision cross section of 10^{-15} cm^2. This altitude is independent of the mean radius R.

Another nonequilibrium correction is necessary because of the finite relaxation zone at the shock front. In this region, the molecular constituents are excited to vibration equilibrium and dissociated by gas kinetic collisions. When the time to relax is long compared to the time it takes a particle to flow along a streamline from the shock front through the shock layer, consideration of nonequilibrium phenomena becomes essential. The radiation from this region may overshoot the corresponding equilibrium value. This is because of the high nonequilibrium translational temperature. At high Mach numbers a strong overshoot of nonequilibrium radiation is observed in shock tubes. This will be discussed in the next section. In Figure A-8 the line labeled "equilibrium", taken from [13], gives the altitude at which the relaxation time is approximately equal to the time it takes a gas particle to pass through the shock layer. It is only below this altitude that the equilibrium predictions of Figure A-7 are correct.

Non-Equilibrium Radiation of Air

The experimental results of [10], [12] and [15] are shown in Figure A-9. It should be mentioned that the total intensity of nonequilibrium radiation, as measured from the one-dimensional flow pattern behind a normal shock in shock-tube experiments and from the three-dimensional flow pattern along the stagnation streamline in the shock layer of a blunt body, should by no means be expected to agree perfectly. Differences must occur because of the different velocity history and, consequently, the different distribution of residence time of the radiating particles as the gas flows downstream from the shock front. The lack of any density dependence shown in Figure A-9 supports the one-dimensional nonequilibrium zone model for normal shock waves which predicts that the total radiation from the zone is independent of free-stream density at a fixed velocity.

Contrary to the nonequilibrium results for air shown in Figure A-9, (where the nonequilibrium gas radiation is independent of density or altitude), a continuous decay with decreasing density is observed on three-dimensional models. This behavior can be explained in a simple manner by considering the radiation distribution in the shock layer as shown in Figure A-10. The figure depicts the change in streamline radiation pattern as a function of streamline position along the shock front and truncation by the corner expansion fan. As the density is reduced, the length of the nonequilibrium zones continuously increases until the time required for the flow along streamlines to reach equilibrium conditions becomes greater than the residence time of the gas in the shock layer. Since progressivly smaller portions of the nonequilibrium zones exist in the low shock layer, the total radiation observed should decrease continuously with density instead of taking on a fixed and constant value.

Truncation by the body velocity field has been observed by [10] during the flight of small models through shocked air. The nonequilibrium zone model of [10] indicates that the density for truncation effects is inversely proportional to vehicle size. Thus, it is unchanged for constant values of $\rho_\infty R$. In other words, the intensity of nonequilibrium radiation remains important at very high altitudes, e.g., 329,000 feet, for the 58.5 foot spherical shell, and 292,000 feet for the 7 foot spherical shell because the product $\rho_\infty R$ remains at about the same value $\sim 8.5 \times 10^{-7}$ lb/ft^2 as for a 1 foot sphere at 256,000 feet or a 0.1 foot spherical model at a density equivalent to 200,000 feet.

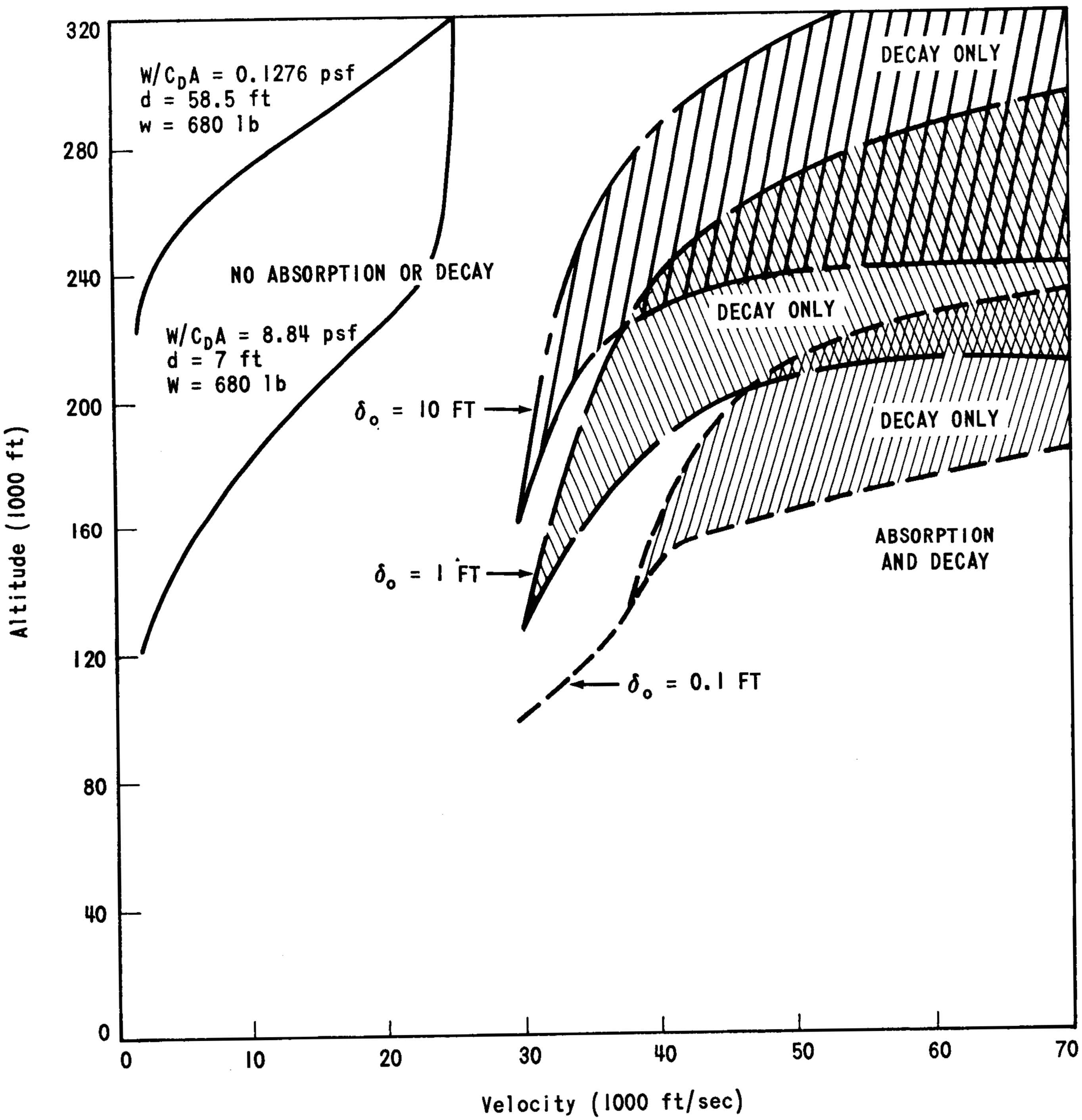

FIGURE A-1 - RADIATION FLIGHT REGIMES

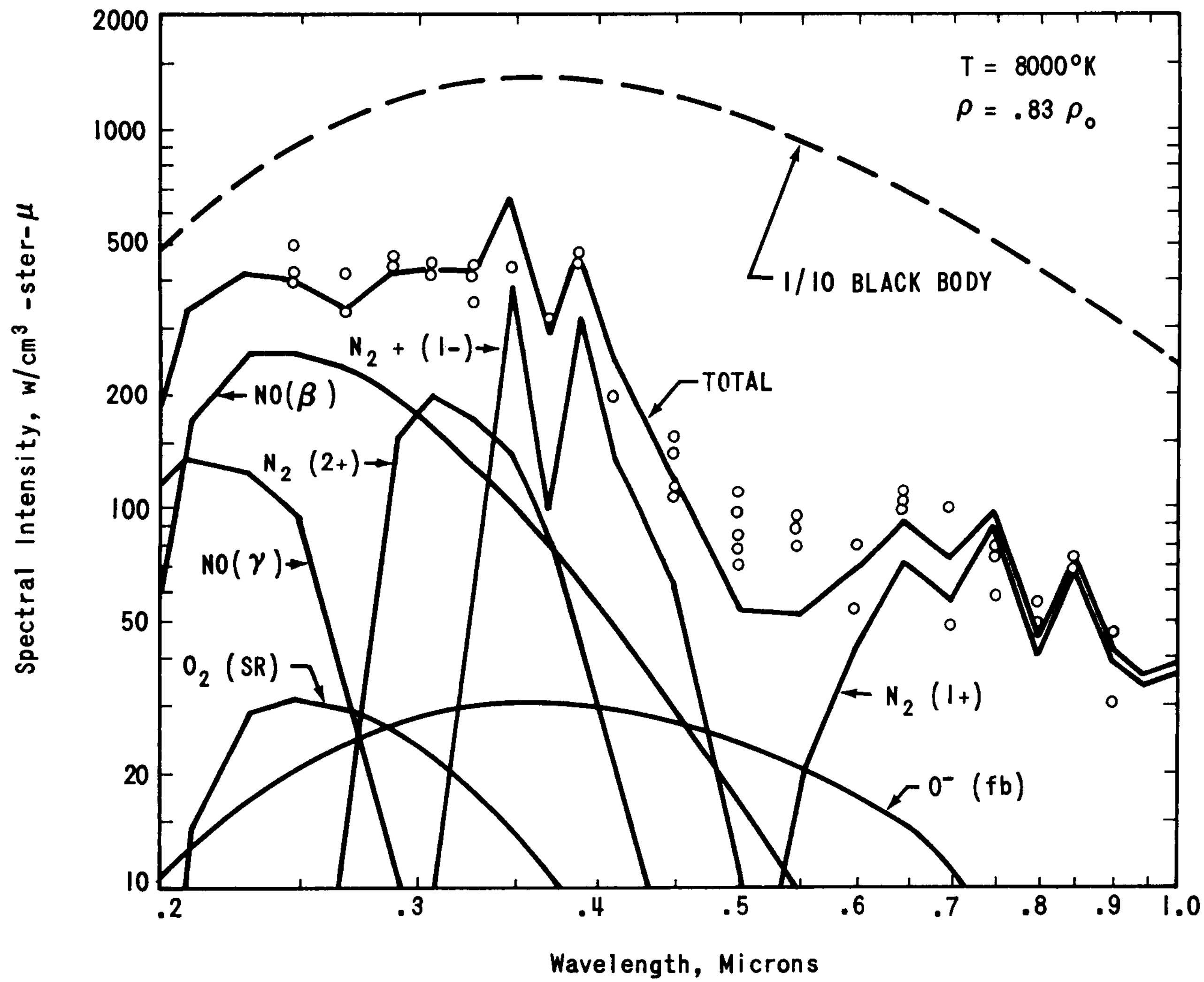

FIGURE A-2 - SPECTRAL INTENSITY OF THE RADIATION FROM AIR (21% O_2 + 79% N_2) HEATED BY REFLECTED SHOCK WAVES AS A FUNCTION OF WAVELENGTH. THE MEASUREMENTS WERE MADE LOOKING ALONG THE TUBE AXIS AND THE EFFECTIVE SAMPLE THICKNESS WAS APPROXIMATELY 1.0 CM. THE CURVES WERE CONSTRUCTED FROM THE THEORY GIVEN IN THE TEXT.

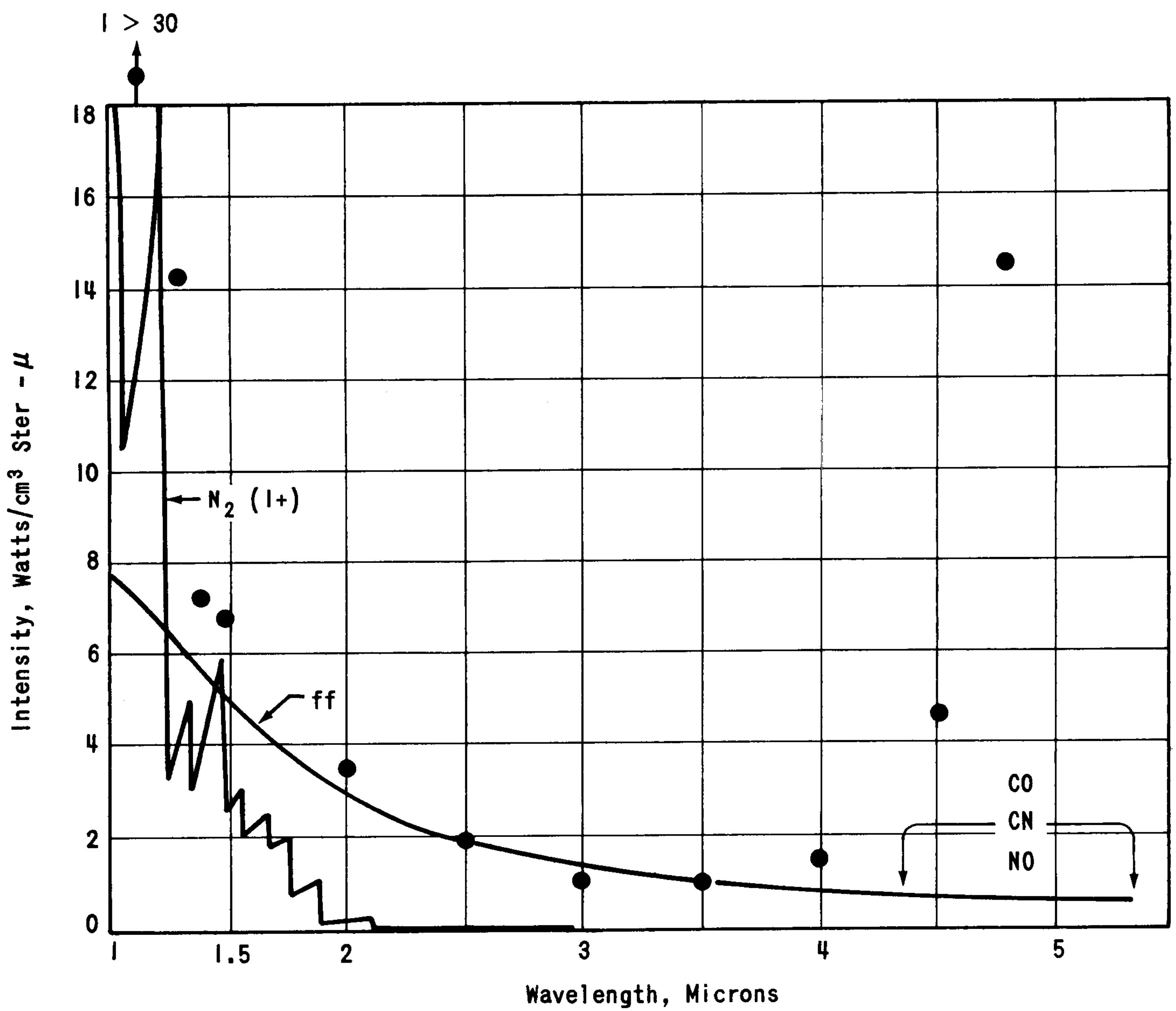

FIGURE A-3 - INFRARED RADIATION FROM AIR AT 8000°K AND 0.85 ATMOSPHERIC DENSITY

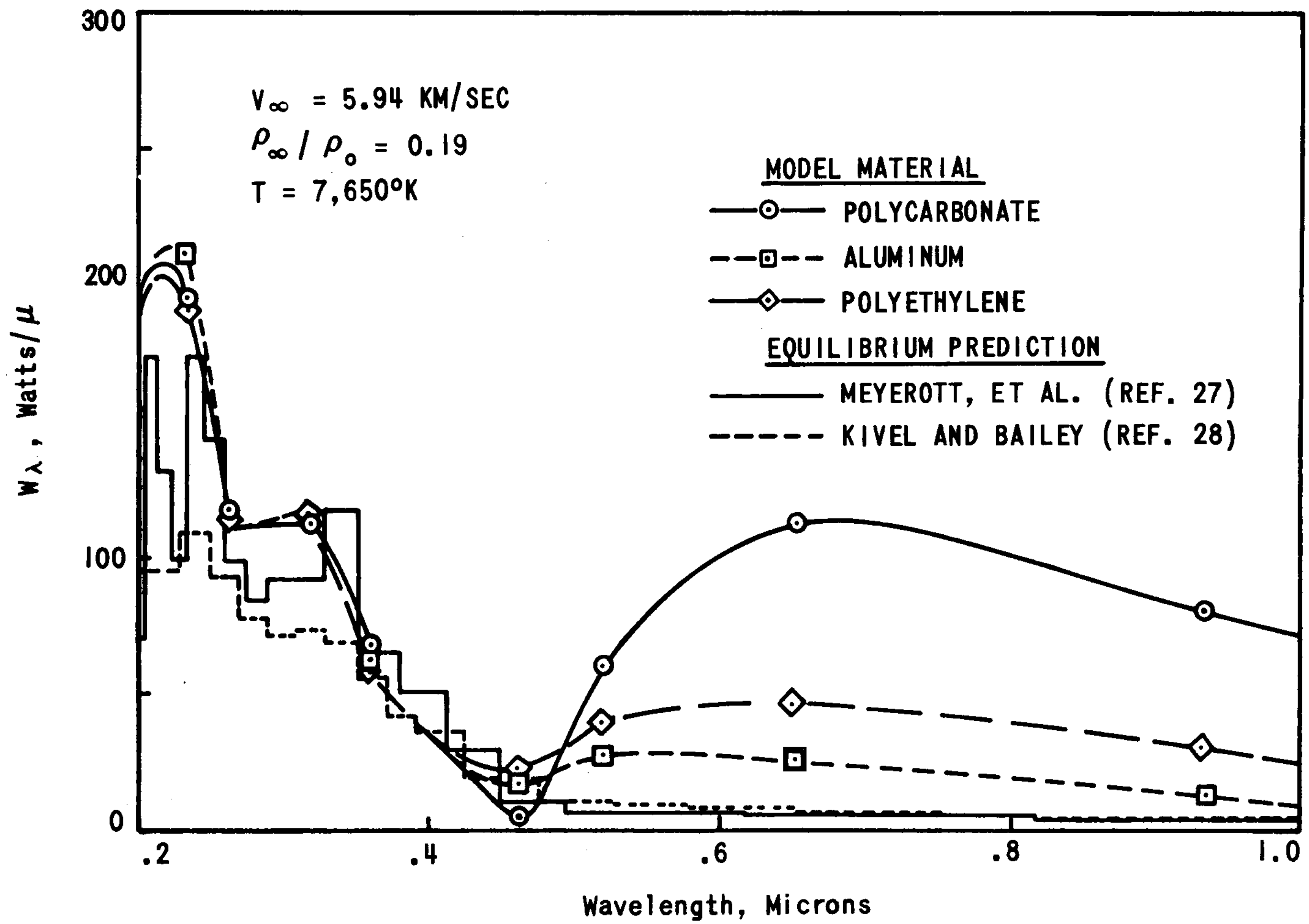

V_∞ = 5.94 KM/SEC
ρ_∞ / ρ_o = 0.19
T = 7,650°K
MODEL MATERIAL
POLYCARBONATE
ALUMINUM
POLYETHYLENE
EQUILIBRIUM PREDICTION
MEYEROTT, ET AL. (REF. 27)
KIVEL AND BAILEY (REF. 28)
300
200
100
0
.2
.4
.6
.8
1.0
W_λ, Watts/μ
Wavelength, Microns

FIGURE A-4a

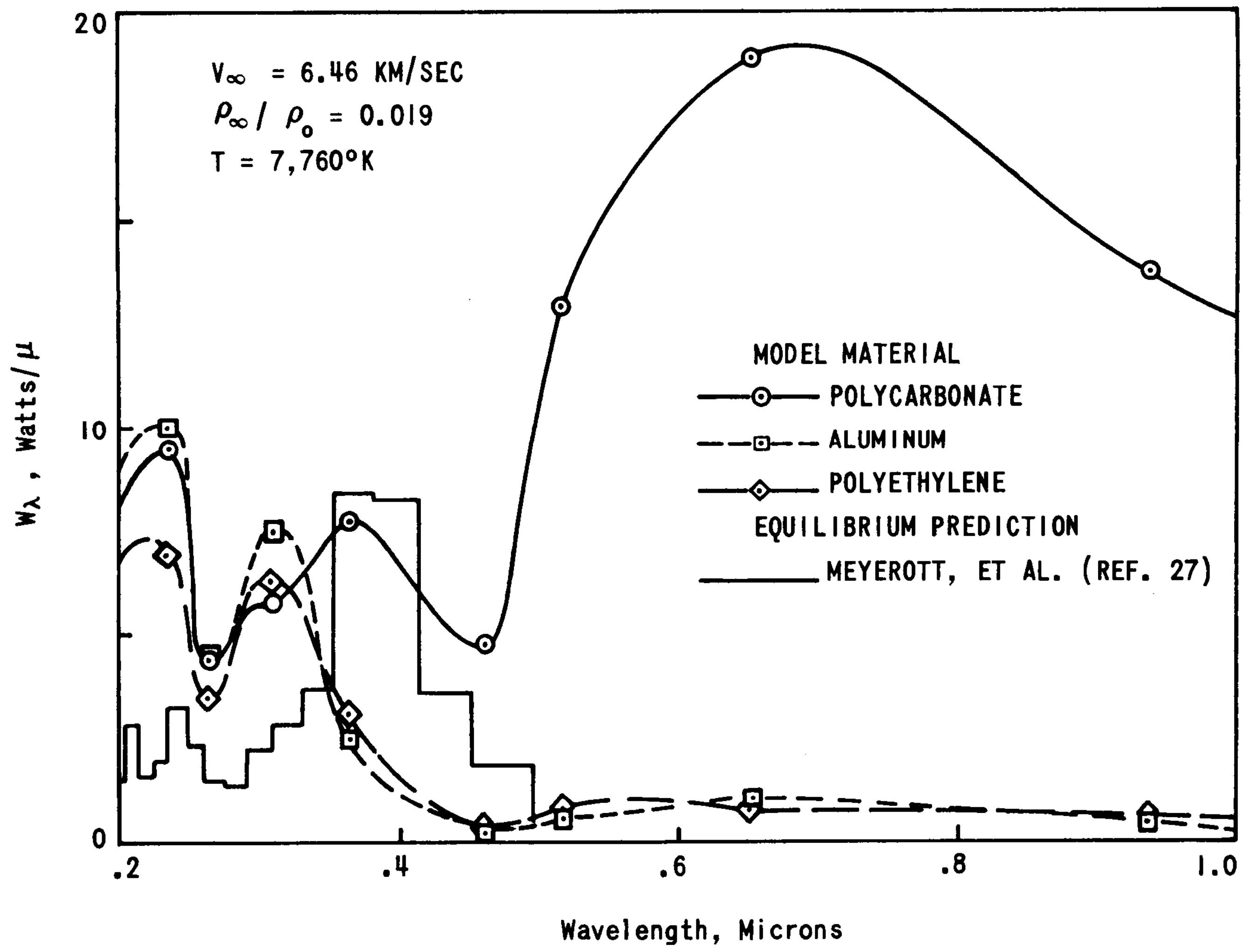

20
10
0
W_λ , Watts/μ
.2
.4
.6
.8
1.0
Wavelength, Microns
V_∞ = 6.46 KM/SEC
ρ_∞ / ρ_o = 0.019
T = 7,760°K
MODEL MATERIAL
POLYCARBONATE
ALUMINUM
POLYETHYLENE
EQUILIBRIUM PREDICTION
MEYEROTT, ET AL. (REF. 27)

FIGURE A-4b

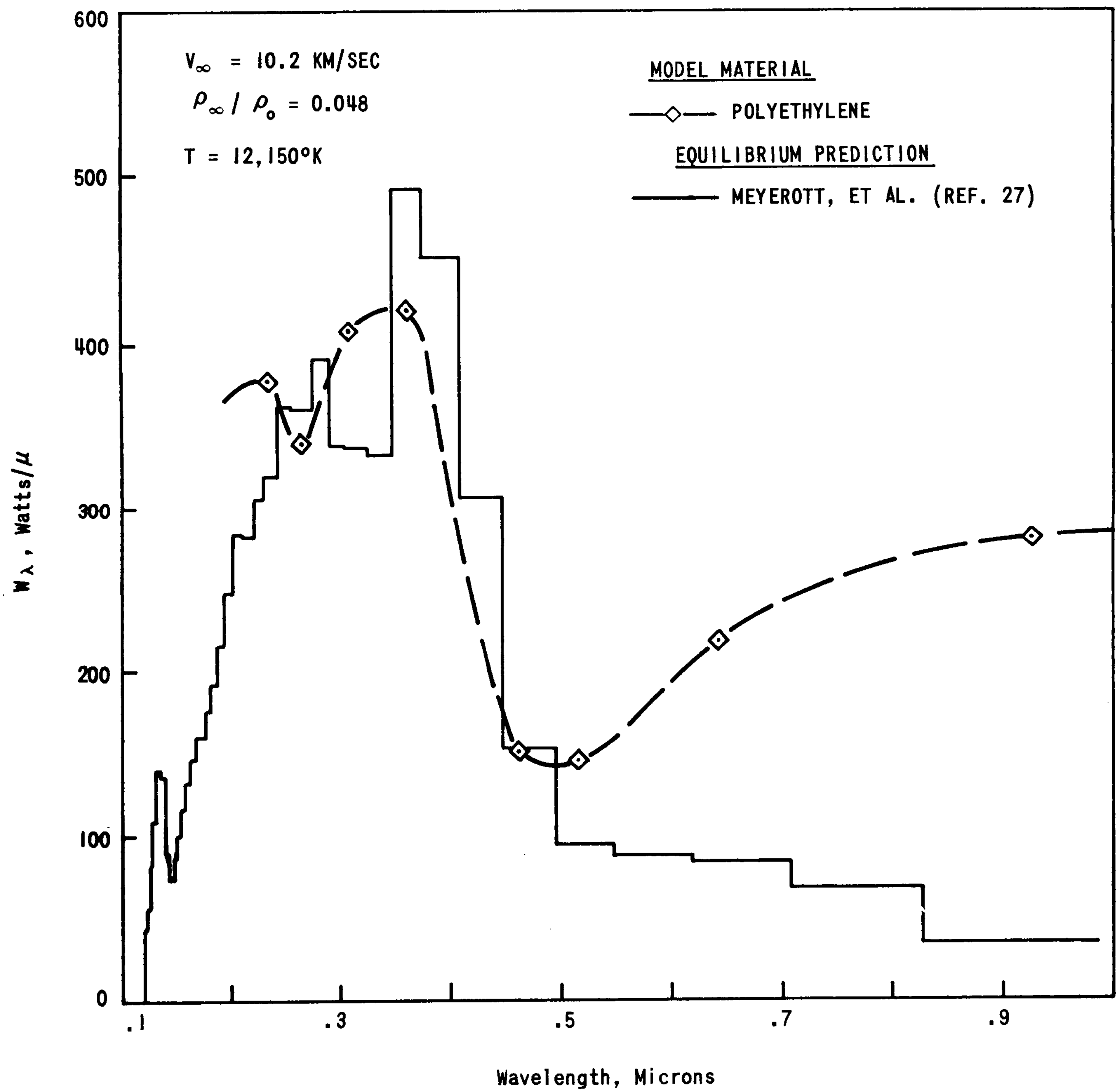

V_∞ = 10.2 KM/SEC
ρ_∞ / ρ_o = 0.048
T = 12,150°K
MODEL MATERIAL
POLYETHYLENE
EQUILIBRIUM PREDICTION
MEYEROTT, ET AL. (REF. 27)
600
500
400
300
200
100
0
.1
.3
.5
.7
.9
W_λ, Watts/μ
Wavelength, Microns

FIGURE A-4c

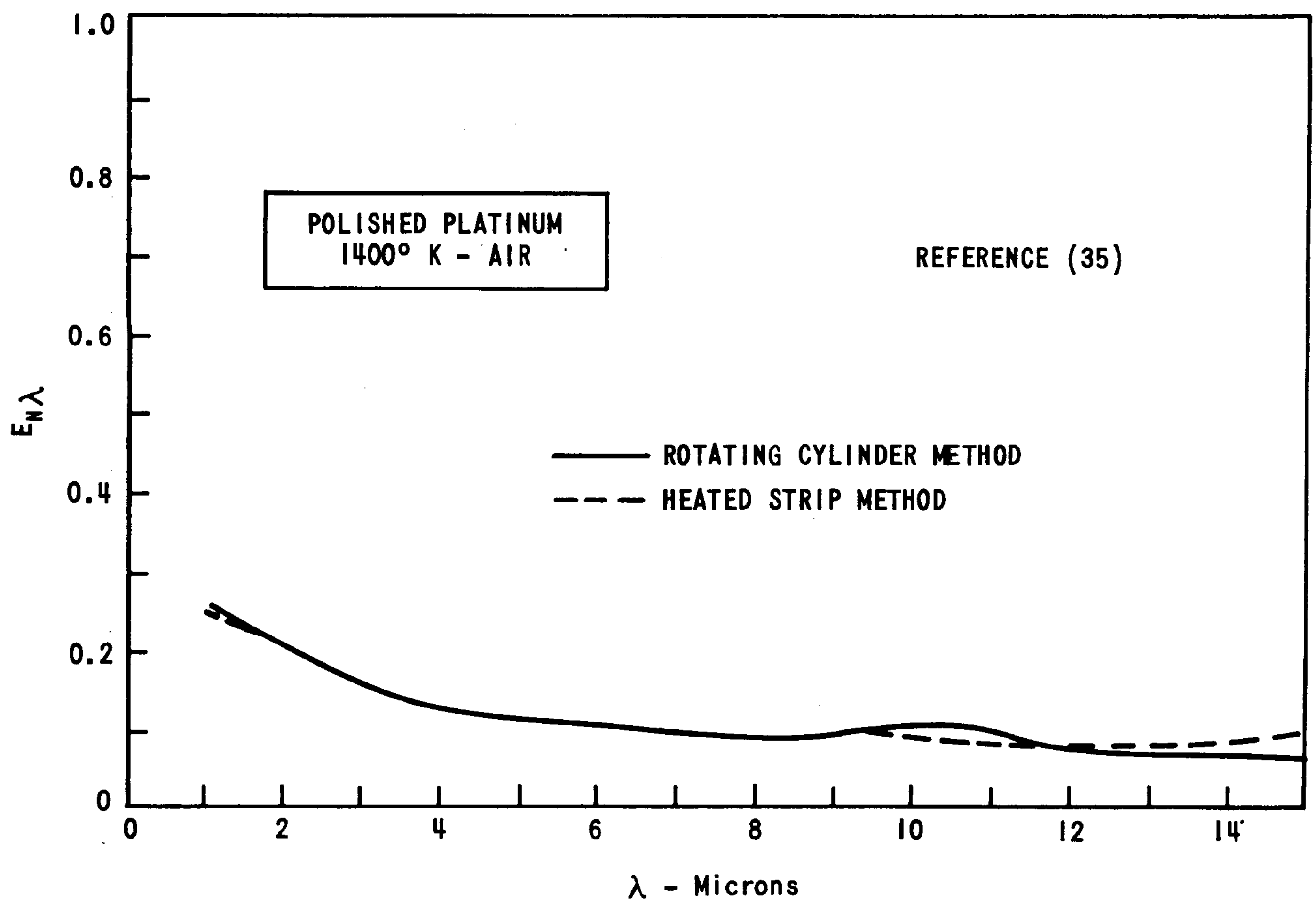

FIGURE A-5 - SPECTRAL EMITTANCE OF POLISHED PLATINUM

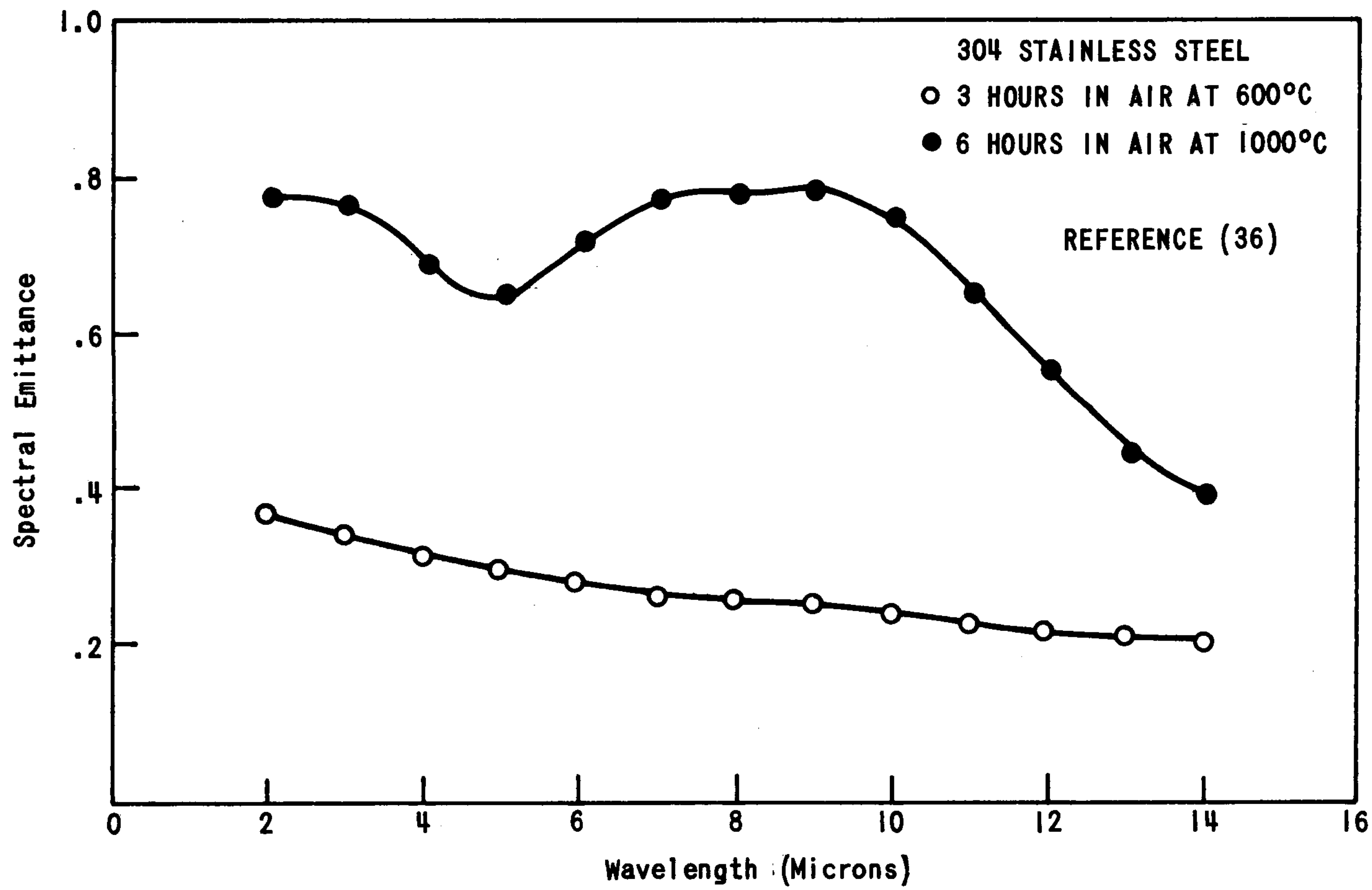

FIGURE A-6 - SPECTRAL EMITTANCE OF OXIDIZED STAINLESS STEEL

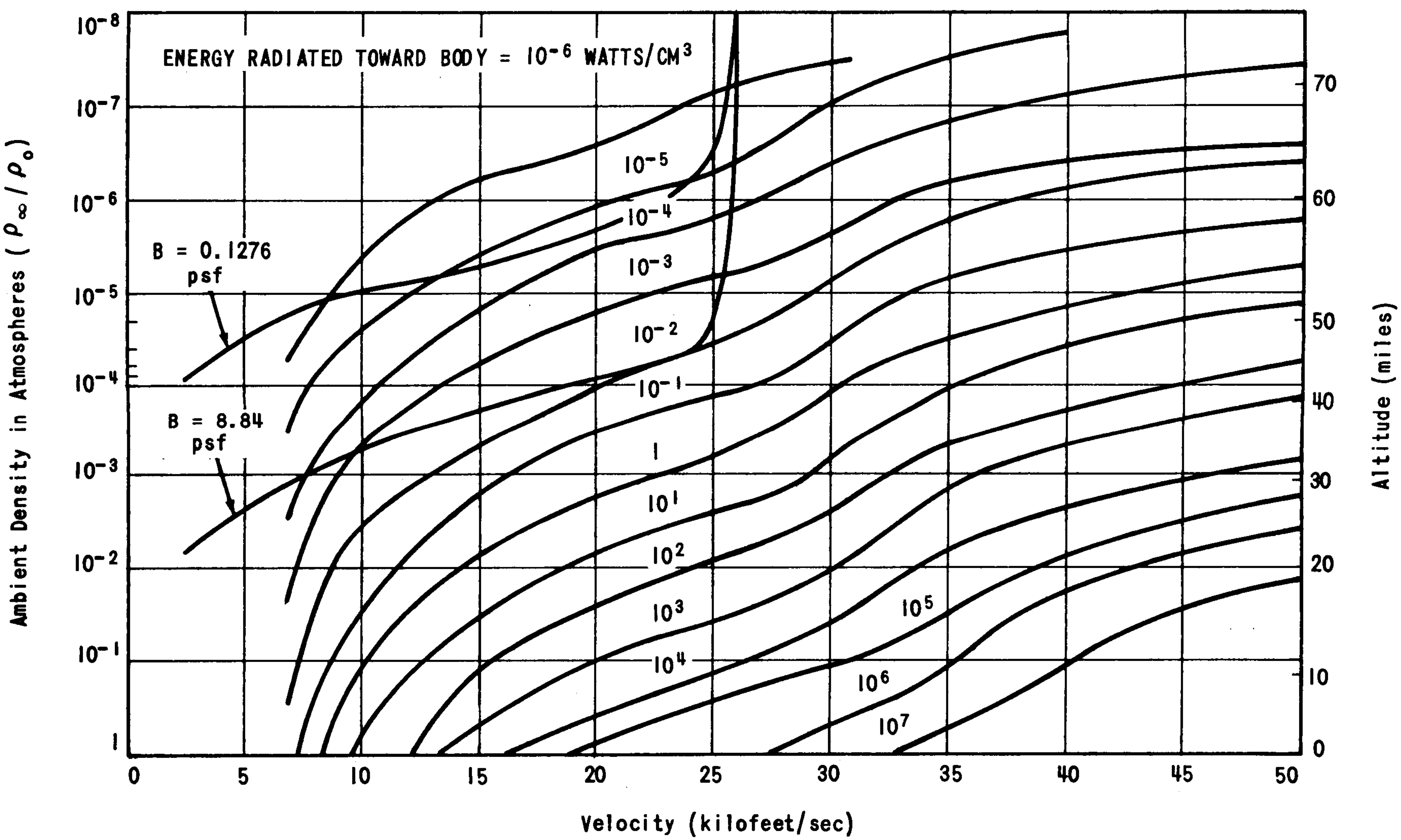

FIGURE A-7 - THE CONTOURS SHOW ONE-HALF ($2\pi I$) OF THE EMITTED RADIATION ENERGY PER UNIT VOLUME FROM THE STAGNATION REGION FOR FULLY EQUILIBRATED AIR. FOR AN OPTICALLY THIN GAS, THIS REPRESENTS AN ENERGY FLUX TOWARDS THE STAGNATION POINT IN W/CM^2 PER UNIT THICKNESS OF GAS CAP.

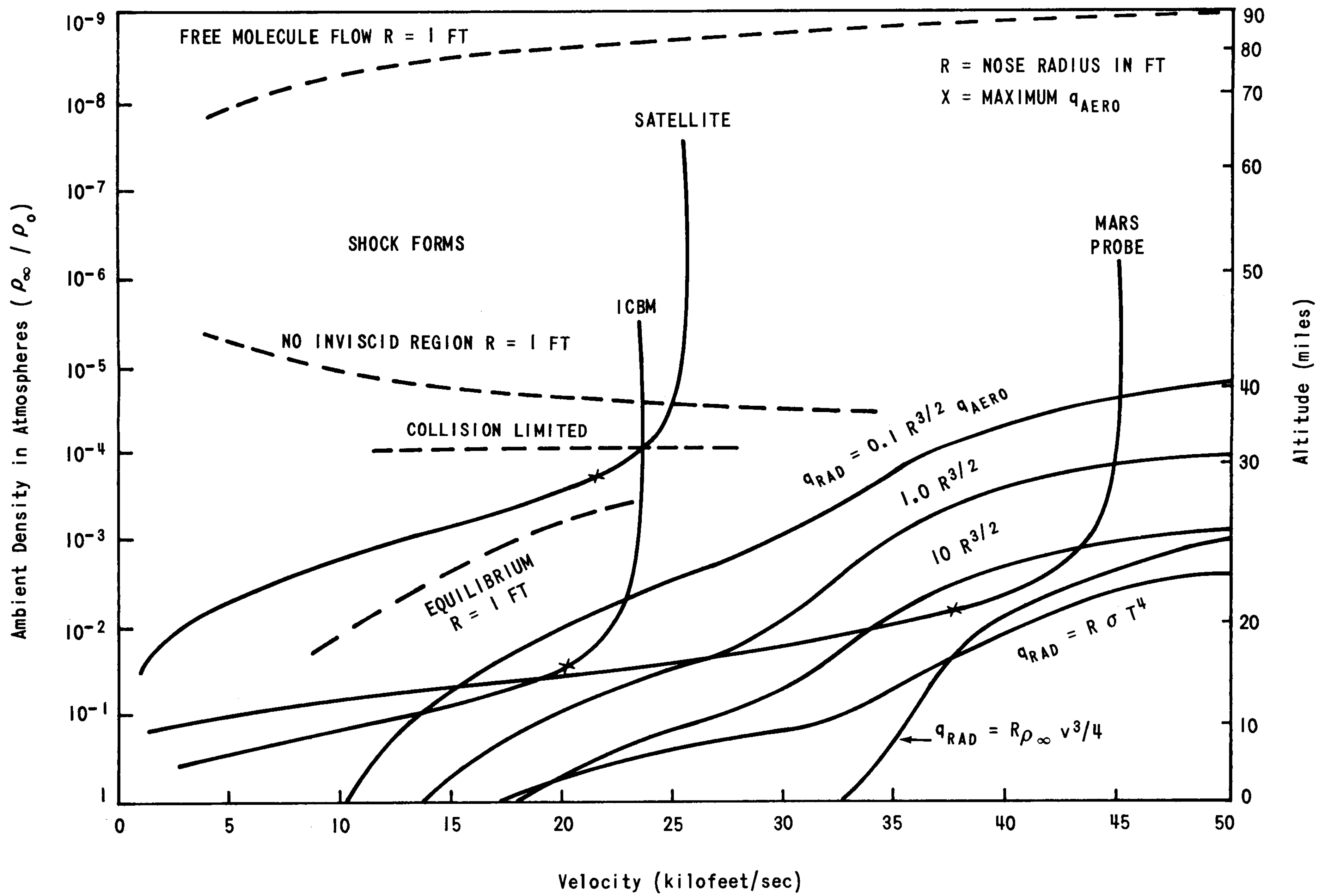

FIGURE A-8 - TYPICAL RE-ENTRY TRAJECTORIES, ALTITUDES AT WHICH NONEQUILIBRIUM EFFECTS BECOME IMPORTANT, AND LINES OF CONSTANT RATIO OF RADIATION TO AERODYNAMIC HEAT TRANSFER

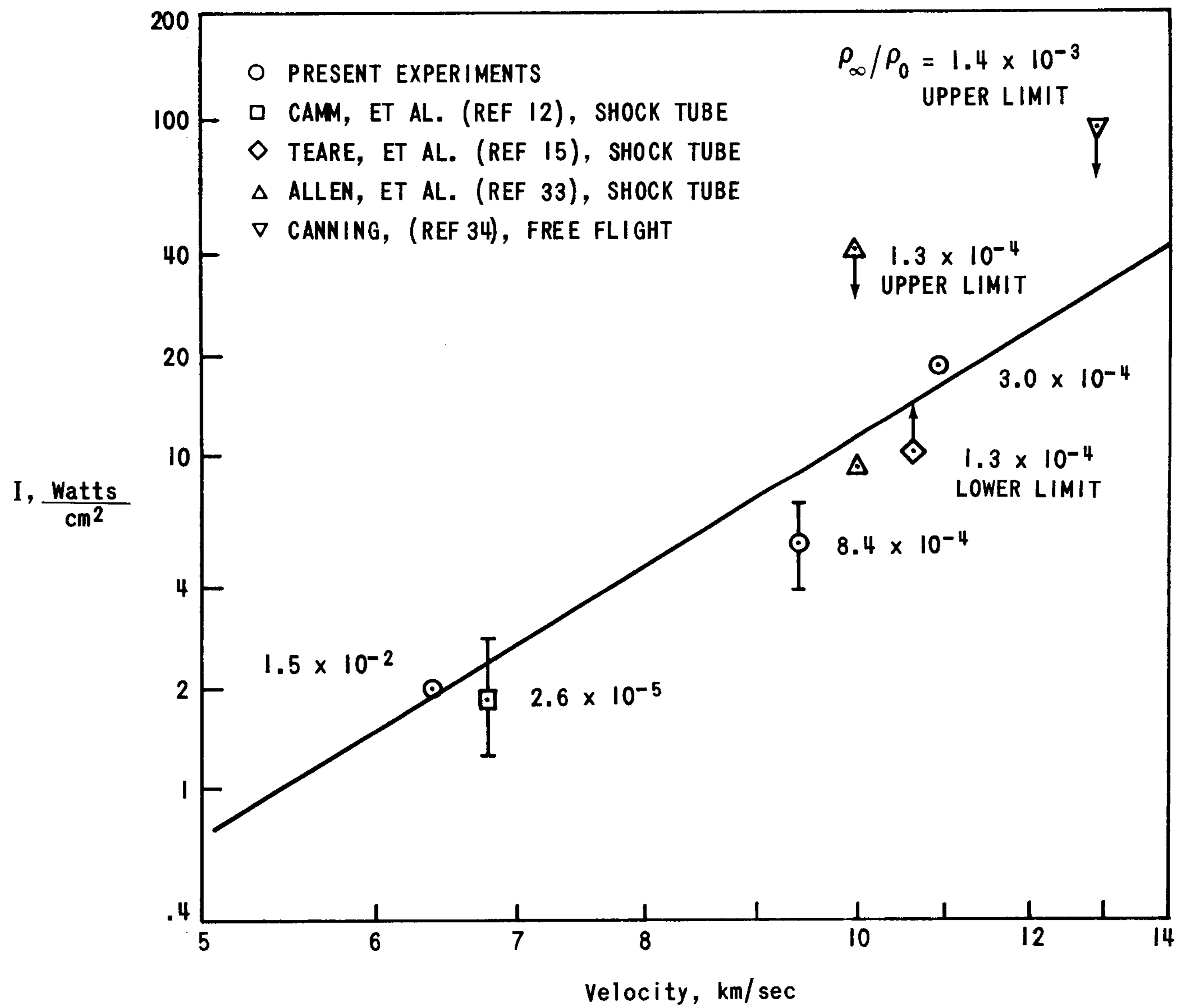

FIGURE A-9 - NON-EQUILIBRIUM RADIATION IN AIR

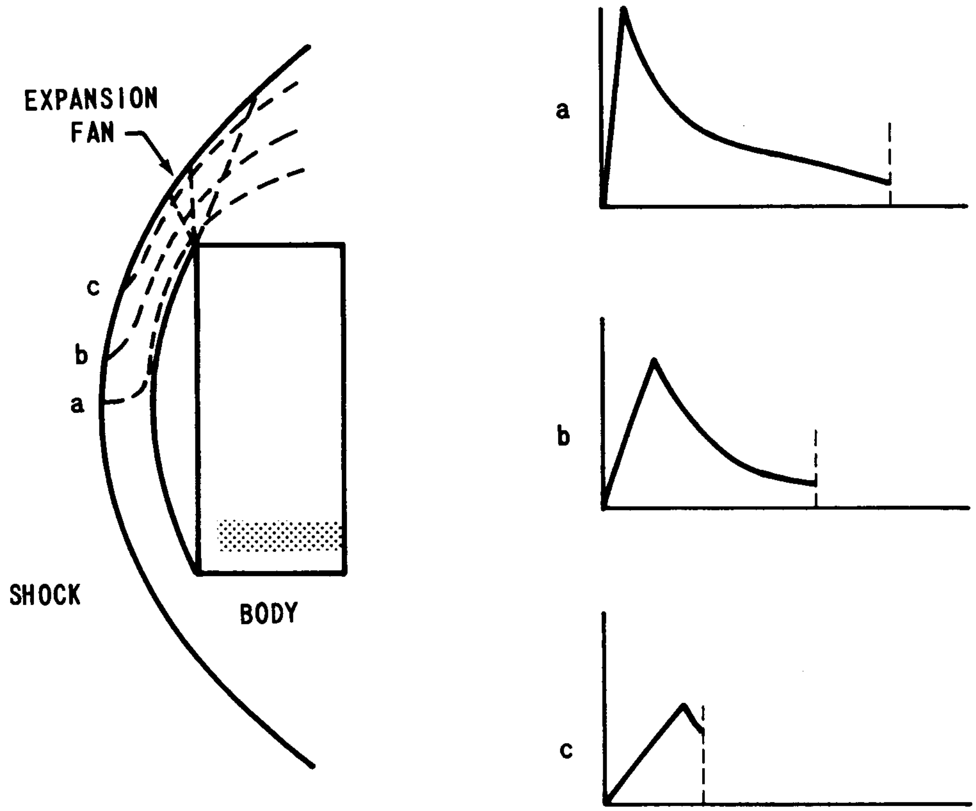

FIGURE A-10 - CHANGE IN THE STREAMLINE RADIATION PATTERN AS A FUNCTION OF STREAMLINE POSITION ALONG THE SHOCK FRONT AND TRUNCATION OF THE RADIATION BY THE CORNER EXPANSION FAN

APPENDIX B - CONVECTIVE HEAT TRANSFER PERTAINING TO REENTRY

Chemical non-equilibrium occurs when finite time is required for the chemical reactions in the gas to take place following large changes in energy levels, as when passing through a strong shock wave. At low flight velocities the chemical reactions, are considered instantaneous and the gas is in "chemical equilibrium". As satellite velocities are approached, the time required for the chemical reaction becomes appreciable; in fact, the gas may pass through the shock wave and over the nose of the entering body without the chemical reaction occuring. This flow condition is termed "chemically frozen". A more formal definition is:

$$\text{Chemical Equilibrium: } \frac{\text{Chemical Relaxation Time}}{\text{Characteristic Flow Time}} << 1$$

$$\text{Chemically Frozen: } \frac{\text{Chemical Relaxation Time}}{\text{Characteristic Flow Time}} >> 1$$

As may be seen in Figure B-1 obtained from [17] there will be an initial portion during entry where the flow regime will be "frozen" for a 1-foot sphere. The reacting zone will be approximately 50,000 ft higher in altitude for a 10 ft nose radius, and another 50,000 ft higher in altitude for a 100 ft nose radius.

The equation of Detra and Hidalgo is based on the theoretical prediction for equilibrium flow of Fay and Riddell, [18] with the additional assumption of a Newtonian velocity gradient at the stagnation point, the gas dynamics charts for equilibrium air of Feldman, [19], the viscosity temperature dependence given by Sutherland, a Lewis number of 1.4 and a Prandtl number of 0.71. Actually, stagnation laminar heat transfer at hypersonic speeds is also dependent on the rate of recombination of the dissociated air (e.g., oxygen atoms to oxygen molecules and nitrogen atoms to nitrogen molecules) at the surface. When the time to recombine is large relative to the time of diffusion (of the molecules, atoms, ions and radicals) across the boundary layer then the atoms, ions and radicals recombine (to N_2 and O_2 molecules) at the wall to a degree dependent on the catalytic behavior of the wall. (This depends on the wall material and flight conditions). In the chemical process of recombining, heat is given off. Thus, in addition, to ordinary heat convection there exists a contribution due to themochemical changes within the gas phase boundary layer and at the gas/solid interface. The Fay and Riddell equation can be modified for the recombination at the wall. This was done by Rosner, [20]. However, since cool metal surfaces at high altitudes are nearly fully catalytic, the catalytic parameter, φ, of [21] tends towards unity, and, therefore, the "fully" catalytic wall equation of Fay and Riddell as correlated for the case of "frozen flow" is applicable. For purposes of comparison with the results previously obtained with the approximate equation for equilibrium flow of Detra and Hidalgo, a sample computation using the Fay and Riddell equation for "frozen flow" is shown below.

$$\dot{q}_s = \frac{0.763}{(Pr_f)^{0.6}} (H_e - H_w) \left(\frac{\mu_w \rho_w}{\mu_e \rho_e}\right)^{0.1} (\beta \mu_e \rho_e)^{1/2} \varphi \left[1 + (Le - 1)^{0.63} \frac{C_e h_R}{H_e}\right] \quad \text{(B-1)}$$

where,

φ = catalytic wall parameter, approaches unity for metals

Pr_f = Prandtl number for the case of "frozen" flow conditions, dimensionless

H_e = enthalpy at outer edge of the boundary layer, Btu/lb_m

H_w = enthalpy of the air at the wall, Btu/lb_m

μ_w = absolute viscocity of fluid at the wall, lb_m/ft-sec

ρ_w = density of air at the wall, lb_m/ft^3

μ_e = absolute viscocity of air at outer edge of the boundary layer, lb_m/ft-sec

ρ_e = density of air at the outer edge of the boundary layer, lb_m/ft^3

L_e = "frozen" Lewis number assumed constant at 1.4, dimensionless

C_e = mass fraction of atoms in mixture at outer edge of boundary layer, dimensionless

h_R = heat of recombination, assumed constant

β = inviscid velocity gradient at the leading edge, 1/sec, may be obtained from

$$\beta = \frac{2V_\infty}{d} \left[\frac{\rho_\infty}{\rho_e}\left(2 - \frac{\rho_\infty}{\rho_e}\right)\right]^{1/2}$$

d = diameter of leading edge, ft

ρ_∞ = ambient, "free stream", density, lb_m/ft^3

V_∞ = flight velocity, ft/sec

A sample computation follows:

V_∞ = 21,600 ft/sec

d = 58.5 ft

$$\left.\begin{aligned}\frac{\rho_\infty}{\rho_{SL}} &= 0.33 \times 10^{-6}\\ \frac{\rho_e}{\rho_{SL}} &= 5.5 \times 10^{-6}\end{aligned}\right\} \quad \frac{\rho_\infty}{\rho_e} = \frac{\rho_\infty}{\rho_{SL}} \times \frac{1}{\frac{\rho_e}{\rho_{SL}}} = \frac{0.33\times10^{-6}}{5.5\times10^{-6}} = 0.06$$

Therefore,

$$\beta = \frac{2\times21,600}{58.5} \left[0.06\ (2-0.06)\right]^{1/2}$$
$$= \frac{2\times21,600}{58.5} (0.1162)^{1/2}$$
$$= 252.5$$

and

$$\beta^{1/2} = \sqrt{252.5} = 15.9$$

Detailed calculations indicate that $\rho\mu$ at the wall is at most five time its value at the outer edge of the boundary layer. The fact that this ratio is raised to the 1/10 power in Equation [B-1) makes the corresponding correction of the order of only 5 percent. Thus,

$$\left(\frac{\mu_w \rho_w}{\mu_e \rho_e}\right)^{0.1} \approx 1$$

$Pr_f = 0.76$

and $(Pr_f)^{0.6} = (0.76)^{0.6} = 0.849$

$H_e \approx H_o = 11,000$ Btu/lb_m

$H_w = 330$ Btu/lb_m, for an assumed $T_w = 1350°R$, as before.

Assume $\varphi=1$ (fully catalytic wall)

$$\left.\begin{aligned}\mu_e &= 0.264/3600\ lb_m/\text{ft-sec}\\ \rho_e &= 0.421\times10^{-6}\ lb_m/ft^3\end{aligned}\right\} \text{ from [22]}$$

Assume Le = 1.4

$$\begin{matrix}\text{Std. heat of}\\ \text{recombination}\end{matrix} \left\{\begin{aligned} h_R\ N_2 &= 14,600\ \text{Btu}/lb_m\\ h_R\ O_2 &= 6,600\ \text{Btu}/lb_m\end{aligned}\right\} \text{ from [23]}$$

$h_R\ C_e = h_R O_2\ (0.2346) + h_R N_2\ (C_e - 0.2346)$ from [21] .

At 8300°R, $h_R C_e$ is approximately,

$$h_R C_e = 6660\ (0.2346) + 14,600\ (0.64 - 0.2346)$$
$$= 1551 + 5920$$
$$= 7471\ \text{Btu}/lb_m .$$

Substituting these terms into Equation (B-1) we get,

$$\dot{q}_s = \frac{0.763}{0.849} (11{,}000-330)\ (1)\ (15.9)\ (0.421\text{x}10^{-6})^{1/2}$$
$$\text{x}\ (0.264/3600)^{1/2}\ (1) \left[1 + (1.4^{0.63} - 1)\ \frac{7{,}471}{11{,}000}\right]$$
$$\dot{q}_s = 0.984\ \text{Btu/ft}^2\text{-sec.}$$

When this convection heating flux is added to the non-equilibrium heating flux of 2.03 Btu/ft -sec. and set equal to the radiation cooling flux we get,

$$0.984+2.03 = 0.24\ T_w{}^4 \ \text{x}\ 10^{-12}$$

and

$$T_w = 1880°\text{R}$$

It is seen that the complexities arising from chemical non-equilibrium and from chemical recombination can be ignored in calculation of the aerodynamic heating of the spheres considered in this paper as the results are almost the same as those obtained by use of the much simpler, approximate method of Detra and Hidalgo.

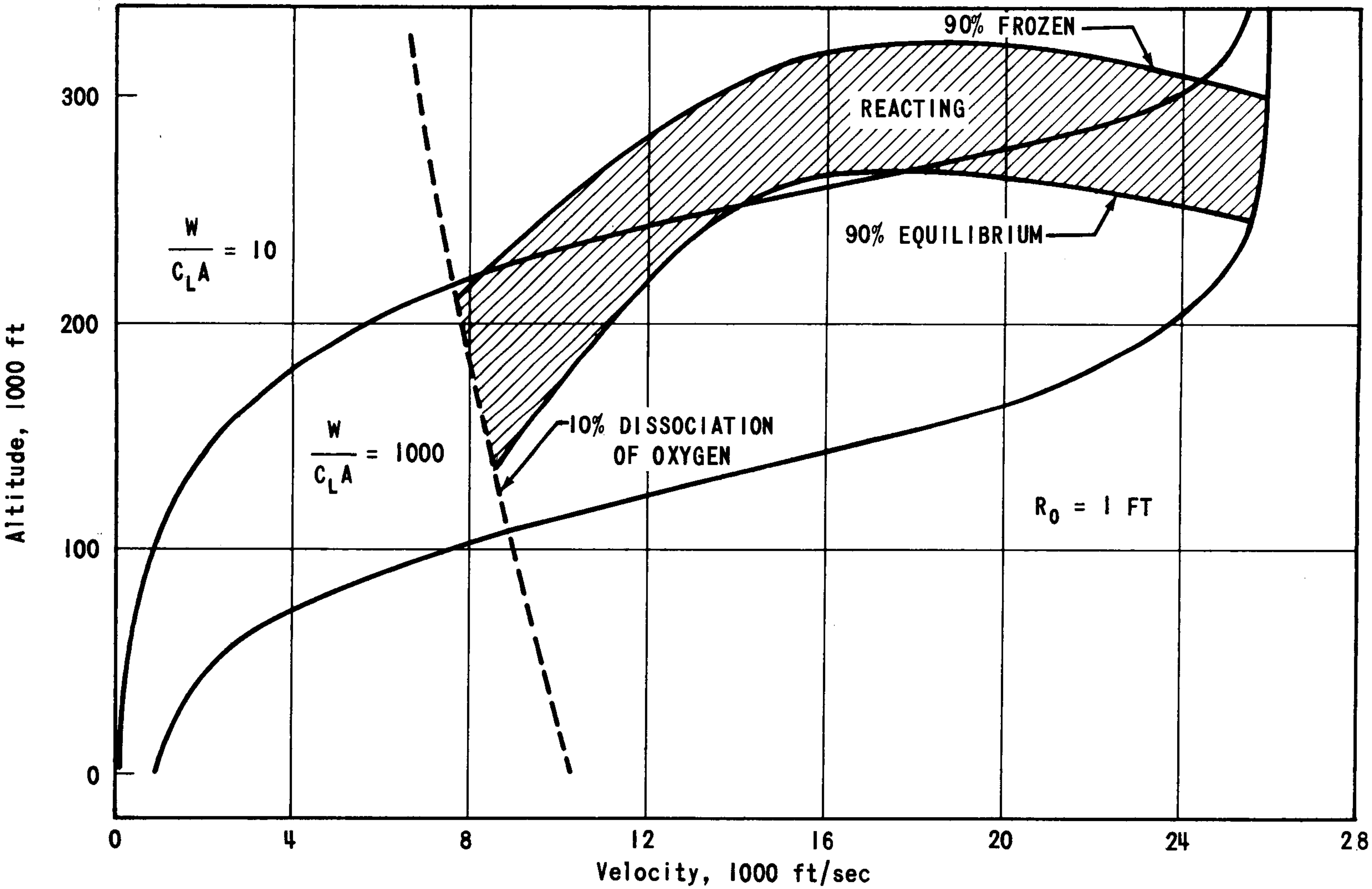

FIGURE B-1 - CHARACTER OF GAS FLOW